JOURNAL OF GEOPHYSICAL RESEARCH, VOL. 106, NO. C7, PAGES 13,879–13,902, JULY 15, 2001

Mesoscale physical and bio-optical structure of the Antarctic Polar Front near 170°W during austral spring

John A. Barth, Timothy J. Cowles, and Stephen D. Pierce

College of Oceanic and Atmospheric Sciences, Oregon State University, Corvallis, Oregon

Abstract. As part of the U.S. Joint Global Ocean Flux Study Southern Ocean program, high-resolution surveys of the Antarctic Polar Front near 170°W were conducted during October-November 1997 with a towed undulating system equipped with conductivity-temperature-depth and bio-optical sensors. Transects along 170°W and two successive mapping surveys revealed zonal bands with sharp meridional gradients in east-west velocity. The Polar Front (PF) was characterized by a sea surface temperature drop from 1.6° to −1.6°C between 60.35° and 61.10°S, with eastward velocities of 0.4-0.5 m s^{-1} in the core of the PF jet. Deep mixed layers (> 200 m) were found within and north of the PF, but mixed layers shoaled to 100-125 m south of the PF to the edge of loose ice at 62.3°S. Highest mixed layer chlorophyll concentrations (0.35 mg m^{-3}) in late October along 170°W were to the south of the PF and associated with cold, fresh water. A large meander of the PF was observed with an alongfront wavelength of 175 km, a cross-front peak-to-peak amplitude of 100 km, and an eastward phase propagation of 0.05-0.08 m s^{-1}, all of which are consistent with its formation via hydrodynamic instability of the PF jet. Highest-phytoplankton biomass was located just poleward of the center of the PF jet. A high-chlorophyll (up to 1.1 mg m^{-3}) 50 by 50 km region was found downstream of the cyclonic bend associated with the meander. A survey 7.5 days later revealed growth of this high biomass region so that chlorophyll was in excess of 0.8 mg m^{-3} over an 80 km cross front by (at least) 80 km alongfront region. High biomass was observed to grow in place with respect to the meander rather than being displaced far downstream as would be expected from advection. This pattern is consistent with meander-driven upwelling of nutrients and/or trace metals, which in turn stimulates phytoplankton growth. Detailed cross sections of the PF reveal narrow 10-20 km wide bands or filaments of phytoplankton biomass that have temperature/salinity properties distinct from surrounding water and are coherent for at least 120 km alongfront.

1. Introduction

The Antarctic Polar Front (PF) is the transition between Antarctic and Subantarctic Surface Waters and is a region of active ventilation of subsurface water. The Antarctic Polar Front Zone is characterized by strong horizontal gradients in density, temperature, salinity, and other oceanographic properties and, as such, is an important boundary when considering Southern Ocean physical, biological, and chemical processes. The PF is associated with a strong eastward current, part of the Antarctic Circumpolar Current (ACC) [*Nowlin and Klinck,* 1986]. The PF exhibits considerable mesoscale variability, as documented by in situ observations [e.g., *Joyce and Patterson,* 1977; *Patterson,* 1985] and satellite remote sensing of sea surface height [*Chelton et al.,* 1990; *Gille and Kelly,* 1996; *Wunsch and Stammer,* 1995] and temperature [*Moore et al.,* 1999a]. *Gille and Kelly* [1996] report spatial decorrelation scales of 85 km for sea surface height variability and assert that the Southern Ocean and the PF, in particular, are regions of intense mesoscale activity. Models of the ACC also show considerable mesoscale activity due to hydrodynamic instability [e.g., *McWilliams et al.,* 1978; *Ivchenko et al.,* 1997].

Several definitions of the PF exist based on strong gradients in sea surface temperature or subsurface properties. Because cold Antarctic Surface Water is plunging beneath warmer Subantarctic Surface Water at the PF [*Gordon,* 1975], a subsurface temperature minimum layer exists. A classic definition for the location of the

Paper number 1999JC000194.
0148-0227/01/1999JC000194$09.00

PF based on subsurface water properties is the northernmost point where the 2°C isotherm passes through 200 m [*Botnikov,* 1963]. In winter this isotherm intersects the surface near the front, but in summer the near-surface waters are warmed, decoupling the surface and subsurface PF signatures. We will use and examine this definition of the PF location in relation to where the subsurface isopycnals slope strongly in association with a strong eastward PF velocity jet.

In terms of its biological importance, elevated surface chlorophyll concentrations in the PF have been found in satellite ocean color data [*Moore et al.*, 1999b]. *De Baar et al.* [1995] report that spring blooms produced phytoplankton biomass in the PF an order of magnitude greater than that in southern ACC waters, presumably because of the greater availability of iron, an important element for phytoplankton growth in the PF region.

Of particular interest to Southern Ocean processes is the degree to which mesoscale processes influence the distribution of heat, salt, nutrients, micronutrients, and plankton within the PF region. More importantly, to what extent do mesoscale physical dynamics influence important chemical and biological processes, including CO_2 uptake, plankton growth, and carbon export [*Flierl and Davis,* 1993; *Moore et al.*, 1999b]?

Recent Southern Ocean expeditions from the United Kingdom and Germany have examined mesoscale aspects of frontal processes in the eastern Pacific sector and the Atlantic sector, respectively. These studies have revealed sharp gradients in physical and biological structure on horizontal scales of 10-20 km [*Pollard et al.*, 1995; *Turner and Owens,* 1995; *Strass et al.*, 2001].

We approached these questions by conducting mesoscale surveys with continuous shipboard acoustic Doppler current profiling and with a towed, undulating package (SeaSoar) that carried high-resolution conductivity-temperature-depth (CTD) and bio-optical sensors. Observations were made during austral spring (October-November 1997) and again during austral summer (January-February 1998) in the western South Pacific. This paper focuses on mesoscale physical and bio-optical patterns and the evolution of those patterns during the surveys in late spring. Our primary objective in this paper is to describe the spatial and temporal scales of variability we observed. We also evaluate a hypothesis for the formation of the observed region of elevated phytoplankton biomass in the PF. Other mesoscale results from this time period are reported by *Abbott et al.* [2000]. A discussion of the initiation of the spring bloom in this region is given by *Landry et al.* [this issue], and a description of the spatial distribution of biological properties from the same mesoscale survey reported here is given by *Brown and Landry* [this issue].

The paper is organized as follows. Section 2 contains a description of the instrumentation and methodology used for the mesoscale survey work. Section 3 presents the results obtained during the multiple transits of the PF with the SeaSoar and quantifies the evolution of a PF meander and its properties. Section 4 explores the implications of the observed variability on our understanding of Southern Ocean processes. Section 5 presents conclusions.

2. Data and Analysis Methods

Hydrographic and velocity data were collected from October 25 to November 19, 1997, using the R/V *Roger Revelle.* This was survey I of the U.S. Joint Global Ocean Flux Study (JGOFS) Southern Ocean study of the Antarctic PF near 170°W. Measurements were collected along a single north-south (N-S) section along 170°W from 58° to 62.3°S and over a 200 by 150 km region centered on the PF near 170°W. Hydrographic data were collected using a towed, undulating vehicle, SeaSoar [*Pollard,* 1986], which cycles rapidly from the surface to depth while being towed at 4 m s^{-1}($\sim$ 8 knots) behind a research vessel. Approximately 3200 vertical profiles were obtained. The SeaSoar vehicle was equipped with a Sea-Bird 9/11-plus CTD instrument with dual temperature/conductivity (T/C) sensors mounted pointing forward through a hole in the SeaSoar nose [*Barth et al.,* 2000]. On top of SeaSoar was a nine-wavelength light absorption and attenuation instrument (Western Environmental Technology Laboratories (WET Labs) ac-9) [*Moore et al.,* 1992] that sampled water pumped from an intake adjacent to the T/C sensors in the nose of SeaSoar [*Barth and Bogucki,* 2000]. The same water supply was pumped through two WET Labs FlashPak fluorometers [*WET Labs,* 1997] mounted alongside the ac-9 on top of SeaSoar. An optical plankton counter for measuring zooplankton size spectra [*Herman,* 1988; *Huntley et al.,* 1995] was mounted on the bottom of SeaSoar. The SeaSoar vehicle also carried an engineering package for real time reporting of pitch, roll, and impeller rotation rate to aid in flight operations. Results from the CTD and the fluorometers are presented here.

During previous experiments with instruments mounted on top of and below SeaSoar and towing the vehicle with 5/16" hydrographic cable equipped with hydrodynamic fairing, maximum sampling depths were 250-300 m [*Huyer et al.,* 1998]. In order to sample more of the deep thermohaline structure in the Southern Ocean a larger sampling range was obtained by equipping the SeaSoar with wings that were 60% larger and had a symmetrical cross section as compared with the standard cambered wings available from Chelsea Instruments Ltd. Although the Australian SeaSoar group has achieved a profiling range up to 600 m with the larger wings (I. Helmond, CSIRO Australia, personal communication, 1997), with the instruments we had loaded on SeaSoar our effective sampling range was 0 to 350 m.

The CTD data were collected by cycling SeaSoar on a faired cable from 0 to 350 m and back to the sur-

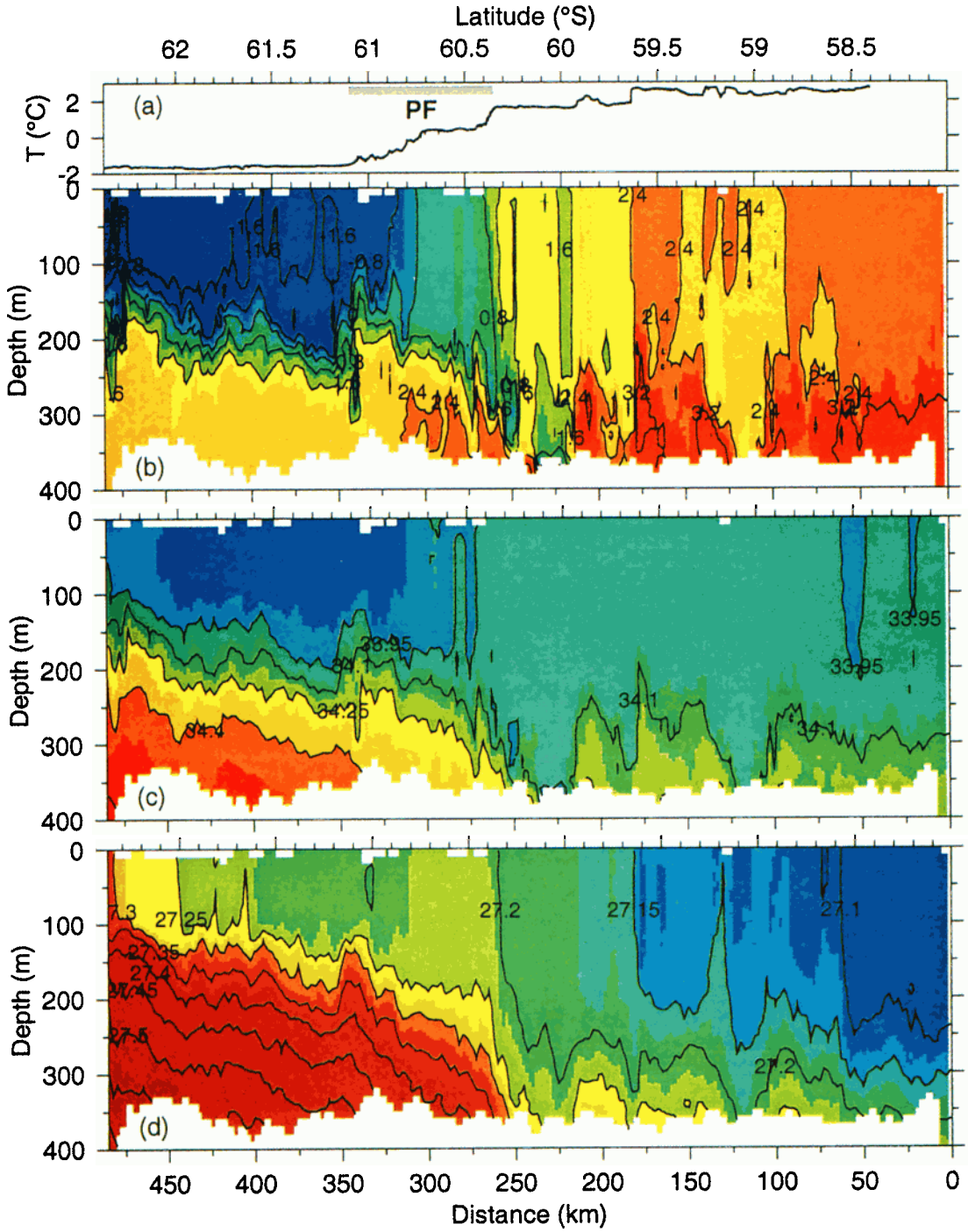

Plate 1. (a) Surface temperature measured from the ship's 5 m underway sampling system and vertical sections of (b) temperature (°C), (c) salinity, (d) density anomaly (kg m^{-3}), (e) shipboard ADCP east-west velocity (cm s^{-1}), (f) chlorophyll with ML depth indicated by a dashed white curve, and (g) buoyancy frequency overlaid with density anomaly contours along 170°W from October 25 to 27 (UTC) in austral spring 1997.

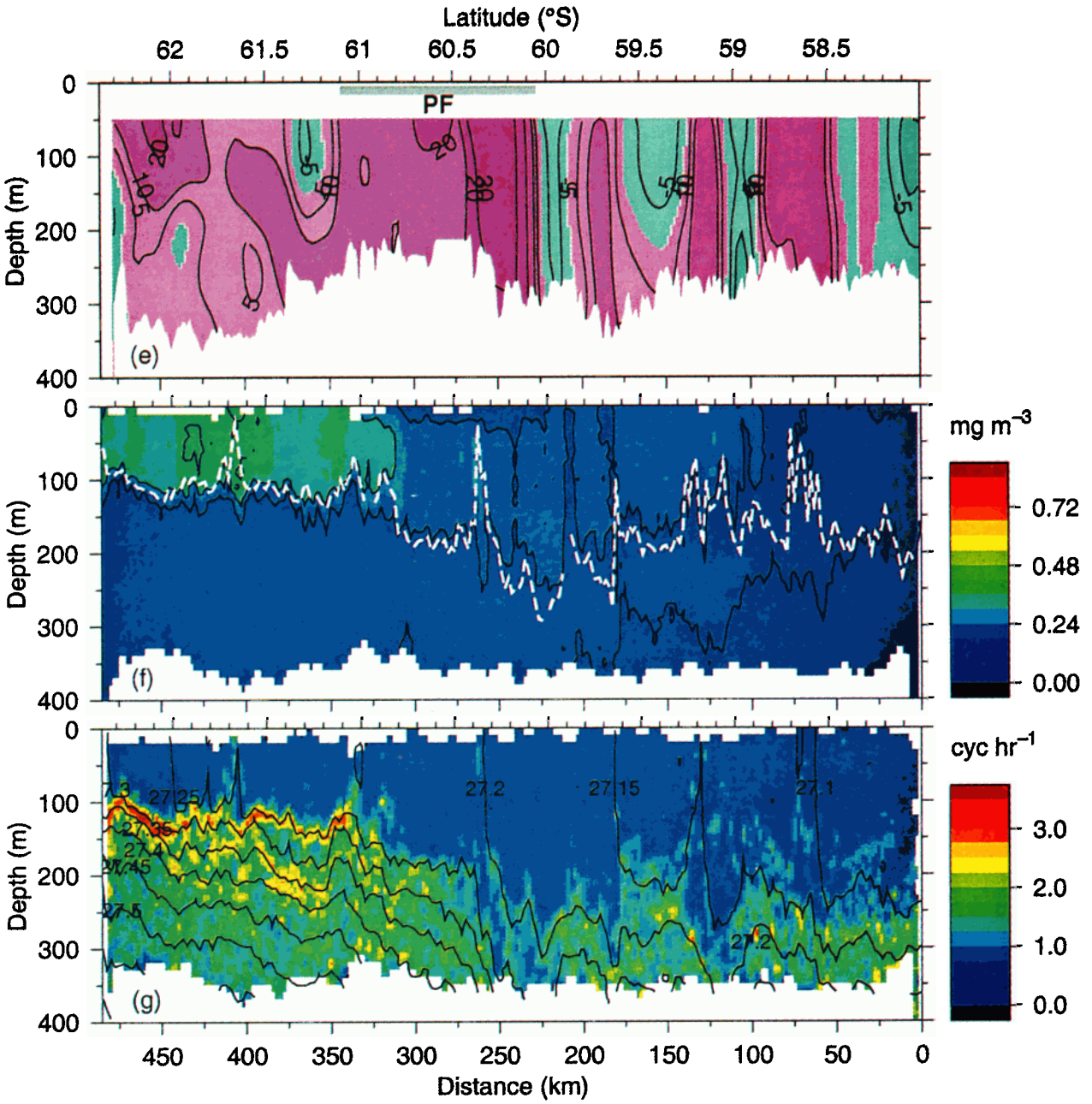

Plate 1. (continued)

face every 8-10 min. The result was hydrographic and bio-optical data with high spatial resolution (2.5 km between along-track surface points, 1.25 km between profiles at middepth) obtained while the ship steamed at 4 m s^{-1}($\sim$ 8 knots). Using time-varying lags and an optimized thermal mass correction [*Barth et al.,* 2000], the 24 Hz temperature and conductivity data were realigned and corrected, used to calculate 24 Hz salinity, and averaged to yield 1 Hz values. The final 1 Hz data files contain latitude, longitude, pressure, temperature, salinity computed using the 1978 practical salinity scale, density anomaly σ_t computed using the 1980 equation of state, date and time. For the depth range of the measurements presented here, differences between density anomaly σ_t and potential density anomaly σ_θ are <0.01 kg m^{-3} and thus negligible. For use in producing vertical sections and horizontal maps, 1 Hz SeaSoar CTD data obtained in a sawtooth-shaped pattern were averaged into 2 dbar vertical bins and 2 km intervals along track. Horizontal maps are contoured using a Barnes objective analysis scheme with two iterations [e.g., *Daley,* 1991], where the grid spacing is 11 km in both directions and the successive zonal and meridional smoothing length scales (unequal because the SeaSoar sampling has higher resolution in the N-S direction) are 20 (9 km) and 13.8 km (6.5 km), respectively.

The spatially averaged temperature, salinity, and pressure data are used to compute geopotential anomaly (dynamic height in meters multiplied by the acceleration of gravity) in J kg^{-1} (m^2 s^{-2}) relative to 275 dbar. Mixed layer depth is defined as the depth at which σ_t differs by 0.01 kg m^{-3} from its surface value. This criterion is a measure of the region of active surface mixing [*Brainerd and Gregg,* 1995].

Fluorescence of the phytoplankton pigments was measured with FlashPak fluorometers [*WET Labs,* 1997] calibrated against extracted chlorophyll pigments obtained from discrete samples and measured with high-performance liquid chromatography. In each FlashPak, light from a xenon flash lamp passes through an interference filter then excites the sample pumped through a quartz flow tube. A photodiode detects the emitted light after it passes through another filter. Both fluorometers were set up to measure chlorophyll fluorescence at 685 nm, but one FlashPak used blue excitation (440 nm, 30 nm bandpass), while the other FlashPak used green excitation (490 nm, 30 nm bandpass). In this paper, we report the chlorophyll content estimated from the fluorescence measured by the "blue" FlashPak. As was done for the CTD data, the chlorophyll values were averaged vertically to 2 dbar and horizontally to 2 km. The estimated uncertainty in the chlorophyll values is 0.03 mg m^{-3}.

Subsurface photosynthetically active radiation (PAR) was measured with a BioSpherical Instruments QSP-200 mounted on the top surface of the SeaSoar vehicle. Surface irradiance values were estimated through extrapolation of near-surface PAR values to the surface using a depth-independent extinction coefficient (K_{PAR}) derived from the light attenuation observed within the upper 100 m. The absence of a sharp vertical chlorophyll maxima and the relatively low chlorophyll levels observed (0.2-0.6 mg m^{-3}) for most of the cruise allowed the determination of a depth-independent K_{PAR} for each SeaSoar cycle during daylight hours. The specific K_{PAR} for each profile was then used to estimate surface irradiance and euphotic zone depth.

Velocity profiles along the ship track were obtained with an RDInstruments hull-mounted153.6 kHz narrowband acoustic Doppler current profiler (ADCP). Measurement ensembles were obtained every 2.5 min using a pulse length of 12 m and a vertical bin size of 8 m. Typical depth range was 300-350 m depending on sea state. A transducer ringing condition degraded the upper few bins; thus the shallowest reliable data were usually at 50 m. For the results presented here the shortest time-averaging interval used is 5 min, for which the inherent uncertainty in the ADCP velocity is <0.01 m s^{-1}. P code GPS navigation (Trimble Tasmin) was used to calculate ship velocity, which was then smoothed using an adaptive local third-order polynomial [*Pierce et al.,* 1999]. Ship's heading was by a combination of gyrocompass (Sperry) and attitude GPS (Ashtech), both recorded at 1 Hz. Calibration to correct for the sensitivity error and the transducer misalignment angle was by the bottom-track method of *Joyce* [1989]; 12 hours of bottom-track data were available at the beginning and end of the cruise during the transit to and from Lyttleton, New Zealand. Ship velocity data are combined with measured ADCP velocities averaged over a layer from 180 to 270 m to determine absolute motion of the reference layer [*Kosro,* 1985; *Wilson and Leetma,* 1988]. The reference layer velocity is then low-pass filtered using a 20 min Blackman window. Finally, the shear profile for each ensemble is added to the reference layer to determine absolute velocity at all depths. The error in absolute velocity due to navigational uncertainty is $\pm$0.03 m s^{-1}.

For maps of ADCP velocities each vector is a 5 km spatial average in the horizontal and 10 m in the vertical. In cases where the cruise track overlays itself, vectors from different times are averaged together. For vertical sections, 5 min ADCP data are contoured using a Barnes objective analysis scheme with two iterations [e.g., *Daley,* 1991], where the horizontal (vertical) grid spacings are 3 km (8 m) and the successive smoothing length scales are 12 (64 m) and 6 km (32 m).

Stream function fields were derived from the ADCP velocities by removing the divergent portion of the velocity field. First, the two components of velocity are gridded using a two-pass Barnes objective analysis [*Barnes,* 1994]. The initial smoothing length scale is 10 km, the final one is 5 km, and the grid spacing is 2 km. Stream function is derived from this gridded

velocity field using the version III method of *Hawkins and Rosenthal* [1965] introduced to the oceanographic community by *Carter and Robinson* [1987]. A Poisson equation for the velocity potential, forced by the observed field of divergence (calculated for each grid box), is solved with a boundary condition of zero on all sides. The resulting velocity potential is then used to add a correction to the boundary conditions for the Poisson equation for the stream function, forced by the relative vorticity field (calculated using line integrals around grid boxes via Stokes theorem, as recommended by *Schaefer and Doswell* [1979]. This approach has the effect of maximizing the amount of kinetic energy in the resulting stream function field. Absolute stream function values are determined by setting the average stream function over the initial 200 by 150 km map to zero. Absolute stream function values for the second map are matched to those from the first by insuring that both maps have the same stream function value at the center of the PF jet.

In this region, tidal currents are expected to be smaller than the subtidal velocity features discussed. The *Schwiderski* [1979] model, for example, shows tidal currents in this region of 0.02 m s^{-1} or less. In addition, removal of the divergent portion of the velocity field through calculation of the stream function reduces the aliasing effects of tidal and other forms of short-term variability.

To analyze the effects of advection, the stream function field is used to advect scaler properties (e.g., chlorophyll) measured over the several days long SeaSoar grids to a common time. The original data are advected stepwise using a 15 min time step. At each step, divergenceless velocity calculated from the stream function using a second-order accurate finite difference scheme is interpolated to the data location and used to advect the data point to the next location. The velocity for each step is obtained from the grid using the improved *Akima* [1996] interpolation scheme, which has the accuracy of a third-degree polynomial. Given the error in absolute ADCP velocity (± 0.03 m s^{-1}), we estimate the error in repositioning the chlorophyll measurements over a maximum of 2.5 days to be about 6.5 km or 0.06° latitude.

3. Results

Winds in late October–November 1997 along 170°W were generally eastward and, during the three SeaSoar sampling activities described here (transect, October 25-27; map 1, November 7-12; and map 2, November 15-19), averaged around 10-15 m s^{-1}(Figure 1). During map 1, wind direction was more variable, starting out westward before swinging around clockwise through almost 360° during the 5 day survey. Winds during map 2 were eastward before weakening considerably toward the end of the 3.5 day survey. Solar insolation was weak during the beginning of each mapping exercise but strengthened through each survey, with notably high values near the end of map 2 (Figure 1).

3.1. North-South Transect Along 170°W

A SeaSoar section south along 170°W (October 25-27, 1997) revealed zonally banded structure in the hydrographic properties and east-west velocity (Plate 1). Sea surface temperature (SST), as measured in the ship's flow-through system, indicated a PF region that extended from 60.35° to 61.10°S, spanning a temperature gradient from 1.6° to −1.6°C (Plate 1a). The two steepest SST gradients occurred between 60.35° and 60.40°S and 60.7° and 60.8°S with a 30 km wide band of 0.25°–0.50°C water between. The change in SST mimics the subsurface temperature variations due to the presence of deep mixed layers (quantified below) after winter mixing. Deep isotherms shoal toward the south and the thermocline is found in the upper 350 m within and south of the PF region (Plate 1b). There is considerable mesoscale structure in the temperature field, in particular, a set of 8-20 km wide cold features within and beneath the PF at 200-350 m between 59.9° and 60.5°S. These features are arrayed along the plunging isopycnal surfaces (e.g., σ_t = 27.225 kg m^{-3}) typifying the PF and suggest the subduction of cold, fresh Antarctic Surface Water to the north beneath the front (Plate 1d). The freshest water, presumably related to recent ice melt, was located 30-100 km north of the ice edge and south of the PF region (Plate 1c).

Currents as measured with shipboard ADCP were eastward throughout the PF region, with the highest values (up to 0.40 m s^{-1} to the east and 0.50 m s^{-1} total speed) on the northern side of the front (Plate 1e). Eastward velocities along the southern edge of the PF region were 0.10-0.20 m s^{-1}, decreasing to the south as the ship approached loose pack ice at 62.3°S. To the north of the PF, alternating bands of east-west velocity are seen.

The hydrographic section obtained with the SeaSoar revealed the mixed layer (ML) extending deeper than 200 m north of the PF region from 58° to 60.3°S (Plates 1b-d). Rapid shoaling of isopycnals (Plate 1d) was observed between 60.3° and 60.4°S, with more gradual shoaling of isopycnals from 60.4° to 62.0°S. A vertical section of Brunt-Väisiälä or buoyancy frequency reinforces this view of MLs (buoyancy frequency less than about 1 cycle h^{-1}) deeper than 250 m north of the PF, deepest ML at the PF, and shoaling of ML to 100-125 m south of the PF (Plate 1g). Estimates of phytoplankton biomass based on calibrated fluorometer measurements from the SeaSoar indicate deep mixing of low concentrations of chlorophyll north of the PF, with some indication of a modest elevation of biomass ($\sim$0.4 mg m^{-3}) at 60.4° and 60.8°S within the PF region (Fig. 1f). Note that the color scale for chlorophyll is chosen to encompass the entire range encountered during the cruise (see below) so as to allow compar-

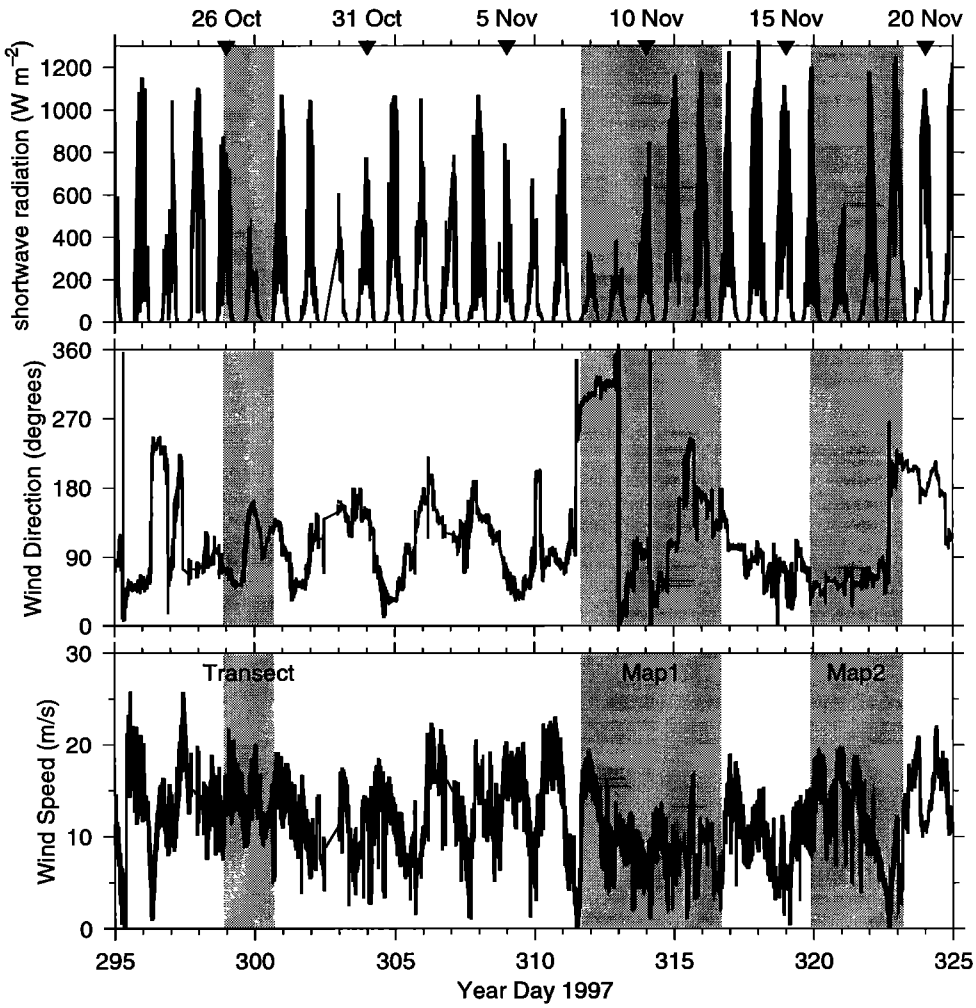

Figure 1. Meteorological time series as measured from the R/V *Roger Revelle*. Wind direction is in oceanographic convention, i.e., the direction to which the wind blows. Shaded bars indicate the timing of three SeaSoar sampling activities.

isons between absolute chlorophyll levels. The highest concentrations of phytoplankton biomass detected on this SeaSoar transect were located between 60.8° and 62.3°S, the southern edge of the transect and the location of the loose pack ice edge (Plate 1b). This region corresponds to the area of freshest water as evident in the salinity section (Plate 1c).

To characterize further the PF, other properties across this region may be examined. Horizontal baroclinic currents are driven by gradients in geopotential anomaly through the geostrophic relationship. That a gradient in geopotential anomaly exists within the PF is evident from the strongly sloping isopycnals (Plate 1d). The geopotential anomaly at 51 m relative to 275 m (we choose these values since the SeaSoar sampling nearly always covered this depth range) across the PF along 170°W is shown in Figure 2a (thick curve). The strongest horizontal gradient occurs where the geopotential anomaly is equal to 1.85 m^2 s^{-2} and coincides with the maximum eastward current (thick curve, Figure 2b). The gradient in geopotential anomaly at 51 m relative to 275 m is a good indicator of the location of the PF front and jet but certainly does not predict the full strength of the jet; that is, a change of 0.3 m^2 s^{-2} across the roughly 100 km wide jet divided by the local Coriolis parameter equal to 1.27×10^{-4} s^{-1} would result in an eastward velocity of 0.02 m s^{-1} compared with the order of magnitude larger measured velocity (Figure 2b).

In order to compare cross-front properties from several N-S sections that cross the PF jet and front roughly orthogonally each section has been shifted in latitude by lining up the location where the geopotential anomaly equals 1.85 m^2 s^{-2} (Table 1). The latitude axis is correct for line 1 of map 1 (see section 3.2 and Figure 3). By lining up the properties in a frontal coordinate system the general structures of the jet and front and their variability can be seen. The SST front occurs over roughly

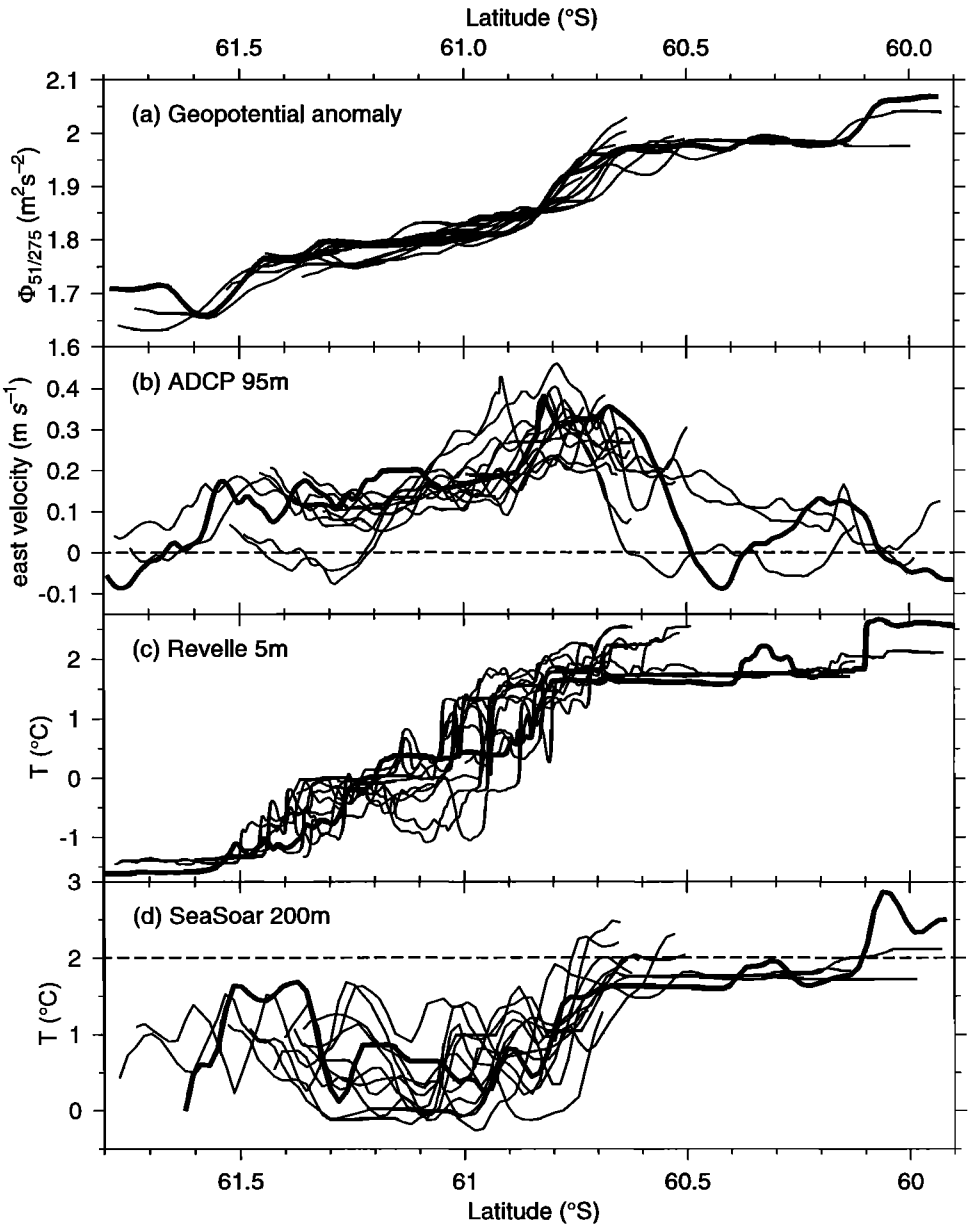

Figure 2. Physical properties across the PF along 170°W (thick curves) and for north-south SeaSoar sampling lines 1-3, 7-9, and 13-18 (see Figure 3 and Plate 2 for locations): (a) geopotential anomaly at 51 m relative to 275 m, (b) Shipboard ADCP east-west velocity at 95 m, (c) surface temperature from the ship's 5 m underway sampling system, and (d) temperature at 200 m. The curves have been shifted to align on the center of the PF as defined by where the geopotential anomaly at 51 m relative to 275 m is equal to 1.85 m^2 s^{-2} (Table 1).

the same temperature range as is found in the initial crossing of the PF and is confined to about 100 km width (Figure 2c). Eastward velocity is elevated within the PF region and generally peaks on the northern side of the SST front region (Figure 2b). The point where the temperature at 200 m is equal to 2.0°C has been used by *Botnikov* [1963] to locate the Antarctic PF [e.g., *Orsi et al.*, 1995]. We found considerable horizontal mesoscale variability in temperature at 200 m (Figure 2d), making it a challenging diagnostic to use. The *Botnikov* [1963] definition would place the PF well north of where the observed SST front, eastward velocity maximum, and strong gradient in geopotential anomaly would place it. The integrating nature of the geopotential anomaly at 51 m relative to 275 m (calculated as the vertical integral of the specific volume anomaly) makes it a better locator of the front.

3.2. Horizontal Variability

Following deployment of current meter and optical moorings between 60° and 61°S [see *Abbott et al.*, 2000], we conducted a SeaSoar survey between 7 and 12 November over the rectangular grid (roughly 200 by 150 km) shown in Figure 3. The nine N-S transect lines

Table 1. Polar Front Location Based on Geopotential Anomaly and Stream Function

SeaSoar Activity	Line	Latitude, °S: geopotential anomaly[a]	Latitude, °S: stream function[b]
Transect		60.37	N/A
Map 1	1	60.83	60.78
	2	60.80	60.79
	3	60.93	60.82
	7	60.22	60.24
	8	60.26	60.26
	9	60.24	60.29
Map 2	13	60.13	60.02
	14	60.20	60.12
	15	60.29	60.21
	16	60.31	60.23
	17	60.43	60.25
	18	60.38	60.32

[a]Defined as the location where the geopotential anomaly at 51 m relative to 275 m is equal to 1.85 m^2 s^{-2}.

[b]Defined as the location where the velocity stream function, derived from shipboard ADCP measurements averaged over 50-100 m, is equal to -30×10^2 m^2 s^{-1}.

comprising this grid (map 1), separated by about 25 km in the E-W direction, revealed a meandering PF, as depicted in a map of SST (Figure 3a). The meander had an alongfront wavelength of ~175 km and a cross-front peak-to-peak amplitude of about 100 km. ADCP velocities averaged over 50-100 m along line 1 to the west of the meander show a Gaussian-shaped jet flowing almost due east centered at 60.83°S (Figure 3b). Deeper velocities (200-300 m average) show a similar pattern indicative of relatively little vertical shear. Downstream of the strong northward bend of the PF, the eastward flow broadened (e.g., line 7).

During this early November survey, higher concentrations of ML phytoplankton biomass (as represented by calibrated chlorophyll fluorescence) were found to the south of the center of the meandering PF and jet, for example, as indicated by the -30×10^2 m^2 s^{-1} stream function contour (Plate 2a). Highest concentrations (up to 1.1 mg m^{-3}) were found in a 50 by 50 km region to the south of the jet near 60.5°S, 168.5°W just downstream of the cyclonic bend. In contouring this field of near-surface chlorophyll, a Barnes objective analysis scheme with minimum smoothing length scales of 13.8 and 6.5 km in the zonal and meridional directions has been used. This leads to realistic contour maps (e.g., no maxima between N-S lines) but serves to smooth out the observed short-scale chlorophyll structure measured along track. To visualize the actual short-scale patterns in chlorophyll, vertical sections of chlorophyll along the SeaSoar lines are presented below.

A second survey of the PF region was conducted from November 15-19 (map 2) with its midpoint being 7.5 days later than that of map 1 (Plate 2b). More details of the physical evolution between surveys are presented below. Phytoplankton biomass was considerably higher in the second survey, with values in excess of 0.8 mg m^{-3} within a region 80 km cross front and (at least) 120 km alongfront. As in the first survey, the high biomass was concentrated to the south of the PF jet axis (-30×10^2 m^2 s^{-1} stream function contour). The center of the high-biomass region during this survey was slightly west (i.e., upstream) of that measured a week previously. This suggests that the location of the high-biomass feature is related to the meandering PF geometry rather than determined by advection of an isolated patch. A more detailed discussion of this is presented below where advection of the chlorophyll features is calculated explicitly.

Details of the cross-front structure along the PF are revealed in a west to east sequence of vertical sections. Along 171.5°W (line 2) the temperature and density

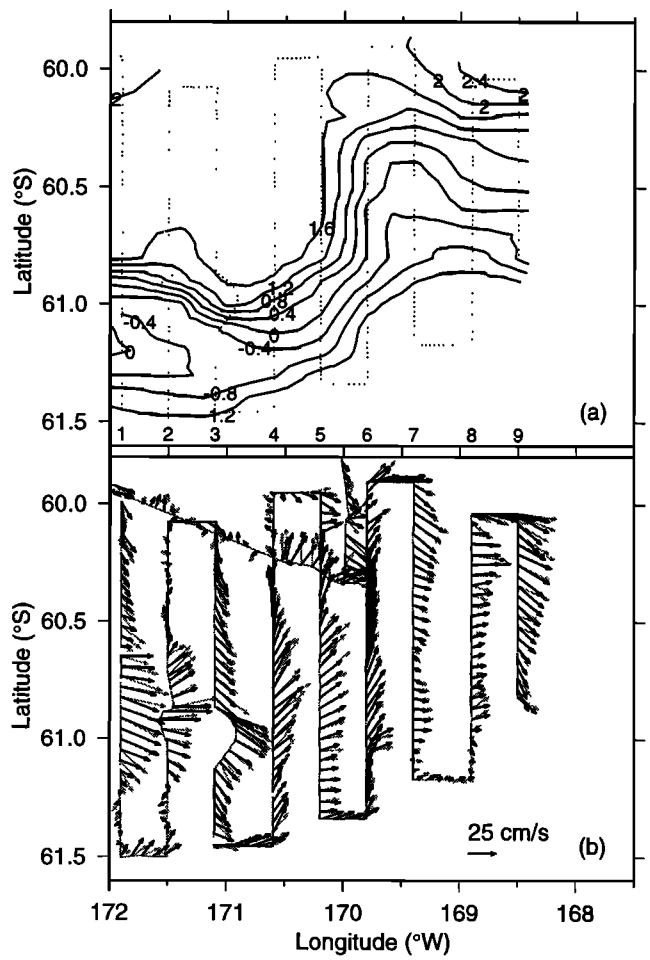

Figure 3. Maps from the first SeaSoar survey, November 7-12, 1997, of (a) surface temperature (°C) and (b) shipboard ADCP velocity averaged for 50-100 m (solid vectors) and for 200-300 m (shaded vectors). Data locations are shown as light dots in Figure 3a, and the ship track is superimposed in Figure 3b. Individual lines are numbered, and a scale arrow for velocity is in the lower left corner of Figure 3b. Note the sharp meander in the PF in both surface temperature and velocity.

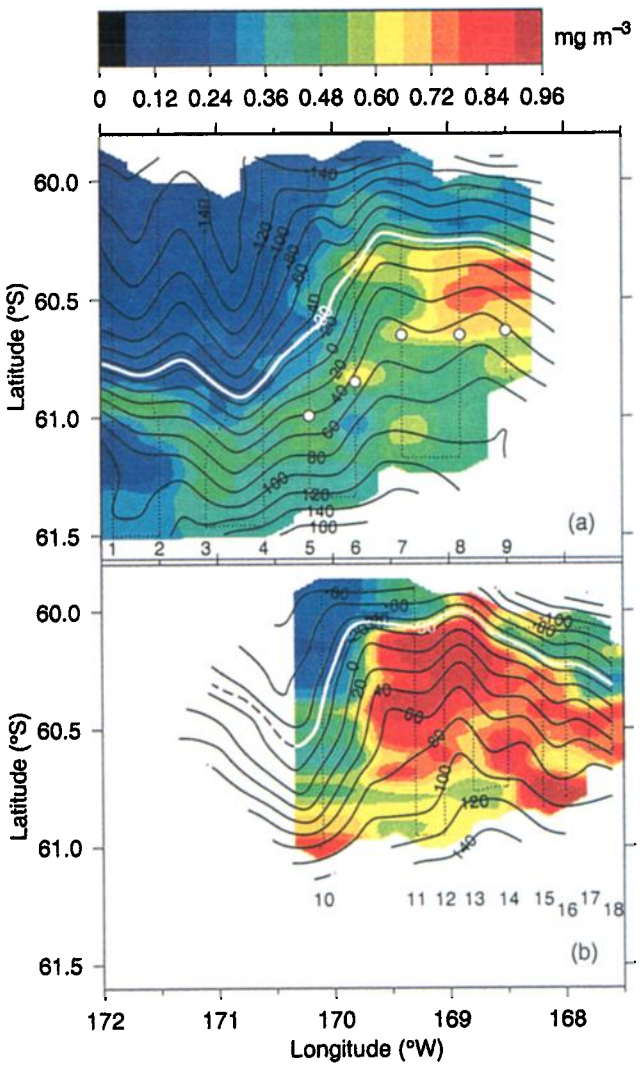

Plate 2. Maps of 51 m chlorophyll (mg m^{-3}) overplotted with contours of velocity stream function (10^2 m^2 s^{-1}) obtained from shipboard ADCP measurements averaged over 50-100 m: (a) November 7-12 and (b) November 15-19, 1997. The highlighted stream function contour indicates the center of the PF jet. White solid circles in Plate 2a indicate the location of a chlorophyll streak along lines 5-9 (see Figure 8a).

structure are similar to that observed along the October 25-27 transect along 170°W, with a surface temperature front near 60.9°S and subsurface temperature variations along density anomaly surfaces (Plate 3). The core of the PF jet (eastward velocity > 0.30 m s^{-1}) aligns with the surface temperature front (−1.0° to 1.2°C). The ML is in excess of 200 m to the north of the PF and is shallower (average depth of about 150 m) within the PF and south. Phytoplankton biomass along the section was enhanced along the southern edge (60.95°S) of the highest-velocity region of the jet (Plate 3c). Chlorophyll concentrations within this narrow zonal band were essentially uniform to depths over 125 m within the ML at that location. To demonstrate the unique characteristics of the band of high-phytoplankton biomass, individual vertical profiles are color-coded by chlorophyll concentration and plotted on a potential temperature θ/S diagram (Plate 4a). From line 2 (171.5°W), profiles are shown from the center of the chlorophyll band (large symbols, Plate 4a) and from 10 km to the north and south (small symbols, Plate 4a). The highest chlorophyll concentrations occur in water with distinct θ/S properties: warmer and saltier than to the south and colder and fresher than to the north where the profile contains a distinct subsurface temperature minimum.

To the east along 169.4°W (line 7) the physical fields were similar to those seen to the west, i.e., maximum eastward velocity (60.0-60.2°S) associated with the SST front of the PF and a relatively shallow (50-100 m) ML within the jet region (Plate 5). There is a clear signature of cold water at depth along isopycnal surfaces (e.g., σ_t = 27.225 kg m^{-3}) below the surface expression of the PF, again indicative of subduction. Phytoplankton biomass (chlorophyll) is higher within a shallower ML than is observed to the west (Plates 3c and 5c). As in the sections to the west, chlorophyll remained organized in narrow bands defined by the flow field and water mass properties. The narrow, isolated, high-biomass feature at 60.65°S (< 10 km wide) was traceable from lines 5-9 (see locations indicated in Plate 2a and further discussion associated with Figure 8). We therefore conclude that this was a narrow "tube" of biomass stretching at least 120 km along the PF. A similar narrow chlorophyll band was observed in the Southern PF in the Bellingshausen Sea near 85°W [*Pollard et al.*, 1995].

As seen to the west at 171.5°W, the θ/S properties of the high-chlorophyll region along 169.4°W (line 7) are distinct from those to the north and south (Plate 4b). High-phytoplankton biomass occurs in a very narrow θ/S range for profiles from within the narrow tube stretching along lines 7-9, confirming the continuity of this feature (line 7, 60.65°S; line 8, 60.65°S; and line 9, 60.60°S; large symbols in Plate 4b). Lower-phytoplankton biomass was found in profiles outside the high-chlorophyll region roughly 25 km to the south in colder, more saline water (line 7, 60.90°S; line 8, 60.80°S; and line 9, 60.83°S; small symbols in Plate 4b). To the north about 50 km, chlorophyll concentration is again low and the θ/S curves show subsurface temperature minima (line 7, 60.17°S; line 8, 60.21°S; and line 9, 60.15°S; small symbols in Plate 4b). The θ/S properties of the high-chlorophyll region are identical to those observed on line 2, confirming the alongfront continuity of this feature as seen in a map of 51 m chlorophyll concentration (Plate 2a). The θ/S properties of the low-chlorophyll water to the north and south are also similar between lines. On line 2 the low-chlorophyll waters were found within about 10 km on either side of the high-phytoplankton biomass band, while on lines 7-9 a span of 75 km was needed to locate similar low-

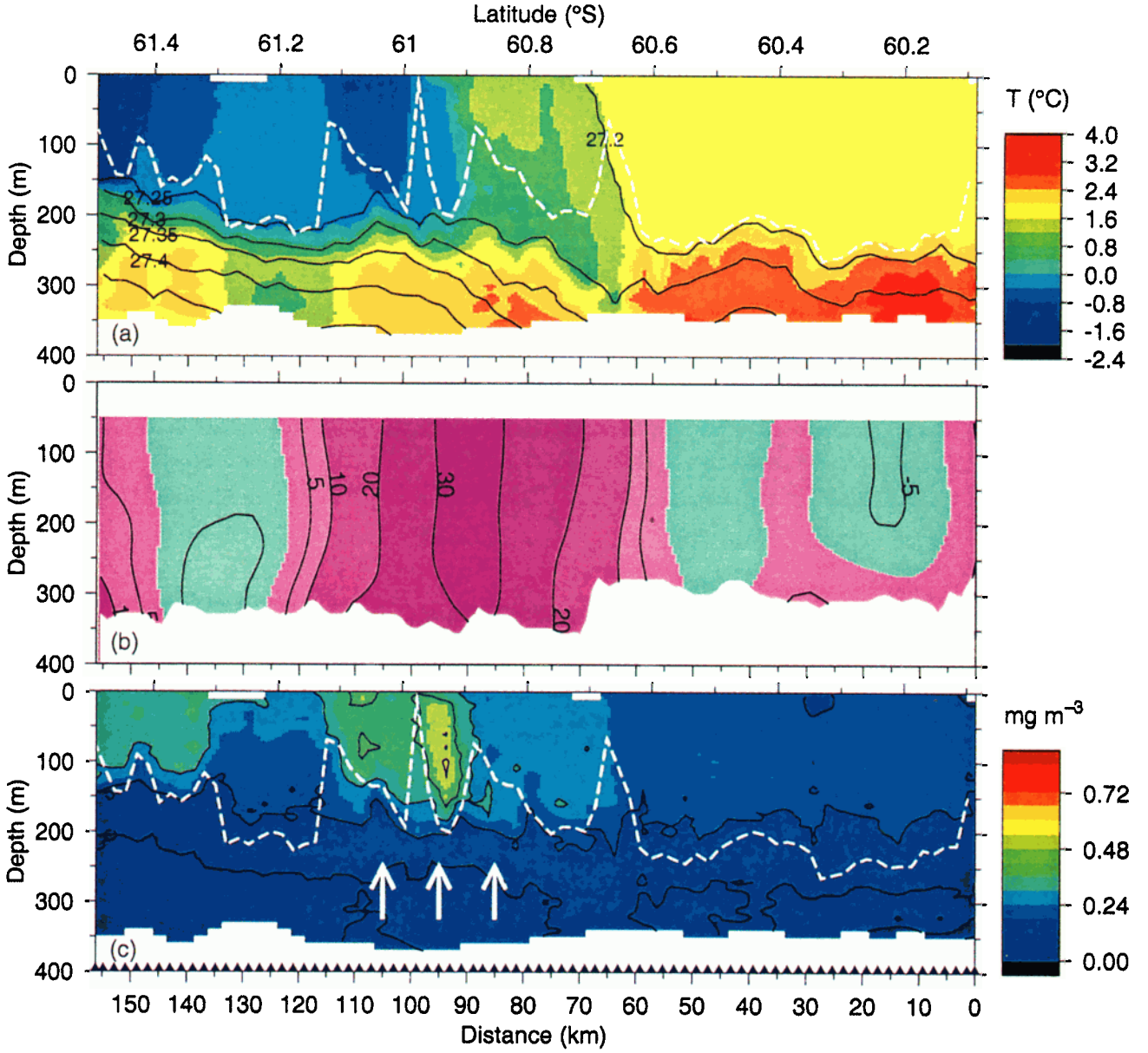

Plate 3. Vertical sections along 171.5°W (line 2) from 0918 to 2143 UTC, November 8, 1997, of (a) temperature overplotted with contours of density anomaly (kg m^{-3}), (b) shipboard ADCP east-west velocity (cm s^{-1}), and (c) chlorophyll. Individual 2 km vertical profiles from the SeaSoar measurements are indicated by solid triangles along the bottom of Plate 3c; ML depth is shown as a dashed white curve. White arrows in Plate 3c show the location of profiles used for T/S analysis (Plate 4a).

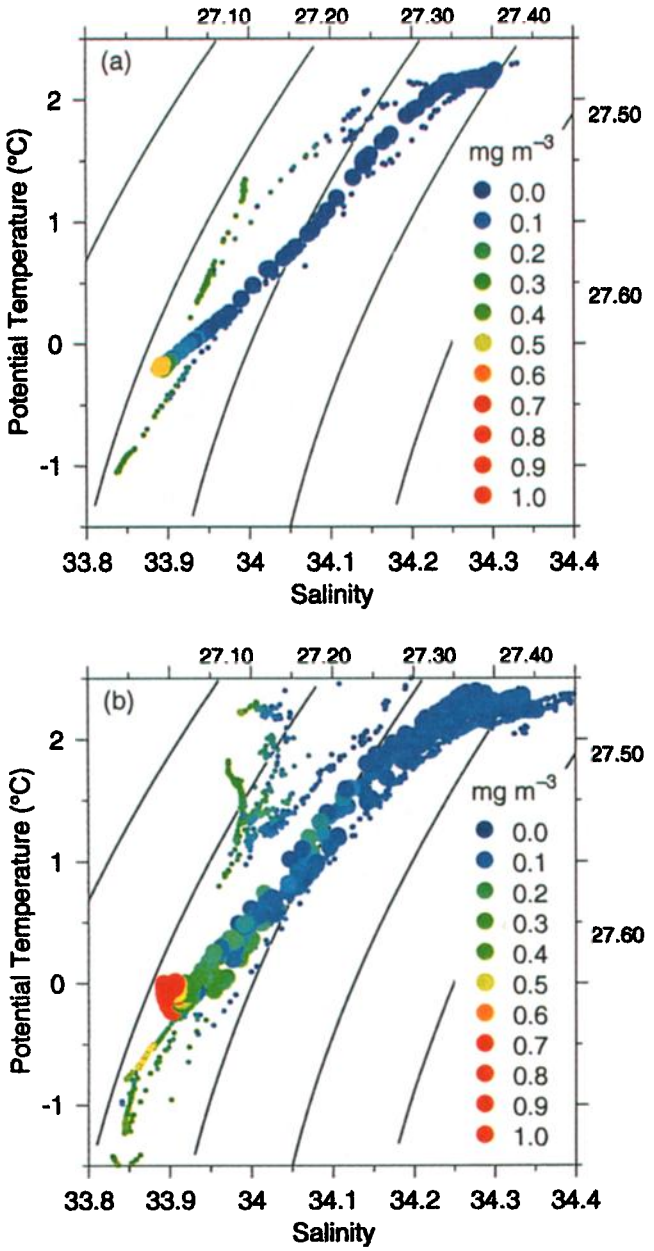

Plate 4. T/S plots color coded by chlorophyll fluorescence from selected profiles along (a) line 2 (171.5°W), November 8, and (b) lines 7-9, November 11-12, 1997. In Plate 4a, large symbols are from within the chlorophyll maximum in the PF, and the small symbols are from 10 km to the north (warmer) and south (colder) (see Plate 3c). In Plate 4b, large symbols are from within the high-chlorophyll feature at the PF, and small symbols are from ~50 km to the north (warmer) and ~25 km to the south (colder) (see Plate 5c).

chlorophyll waters. This increase in latitudinal extent is due primarily to broadening of the PF jet from west to east as evident in the map of ADCP stream function (Plate 2a). The greater than twofold increase in latitudinal extent of the high-chlorophyll region downstream is mainly due to this broadening, not to horizontal diffusion, although diffusion is certainly not zero. The presence of distinct chlorophyll streaks or tubes along the jet (see further discussion below and Figure 8) rather than a homogeneous region of high biomass is further evidence for the minor role of horizontal diffusion in the downstream spatial growth.

Farther to the east along 168.8°W (line 13) within the high-phytoplankton biomass feature observed during the second survey (Plate 2b), the physical structure is again quite similar to that seen upstream (Plate 6). High-chlorophyll concentrations were found within the 100 m ML south of the PF, with a sharp boundary at 60.0°S, coincident with the temperature front and high-velocity jet. Near the PF from 60.1°S and north, however, a tongue of high chlorophyll was discernible down to 200-250 m. This feature was consistent with the presence of cold water beneath the surface front along the sloping isopycnals (e.g., $\sigma_t = 27.225$ kg m^{-3}), consistent with subduction of Antarctic Surface Water to beneath the PF (Plate 6a). The phytoplankton distribution continued to display banded structures across the PF region, with horizontal scales of 10-15 km (Plate 6c).

Note that the phytoplankton biomass within the mixed layer can be represented by the concentration found near 50 m (Plates 3, 5, and 6). Subsequent discussion will refer to the 51 m chlorophyll concentration (based on calibrated fluorescence) as an index for phytoplankton biomass in the mixed layer.

The second SeaSoar/ADCP survey (November 15-19) showed that the meander in the PF jet was still evident in SST and ADCP velocity (Figure 4). Peak eastward velocities were near 0.35 m s^{-1}, and very little vertical shear was evident. Note that additional ADCP data were available to the west of the SeaSoar grid as measured during hydrographic station sampling. These additional data allow ADCP stream function to be derived for a larger region than that covered by the SeaSoar data.

ML depths varied across the PF region as seen in the vertical sections (Plates 1, 3, 5 and 6). Maps of ML depth overplotted with contours of ADCP stream function reveal deep mixed layers (>200 m) to the north of the PF, in particular, to the NW of the anticyclonic meander in the PF jet (Figure 5). ML depth was 140 m or less through most of the remainder of both survey regions, i.e., within the PF jet and to the south. There is a strong correlation between the location of elevated chlorophyll (>0.4 mg m^{-3}) within the ML and ML depths $\lesssim$200 m in both surveys (Plate 2 and Figure 5). Within the regions with ML depth <200 m, however, there is no obvious correlation between ML depth and phytoplankton biomass. A plot of chlorophyll at 51 m versus ML depth confirms that higher biomass was found for ML depths $\lesssim$200 m but that no obvious relationship was seen between these two variables at shallower ML depths (Figure 6a). ML depth is often related to the strength of the surface wind speed, but during these surveys there was no functional re-

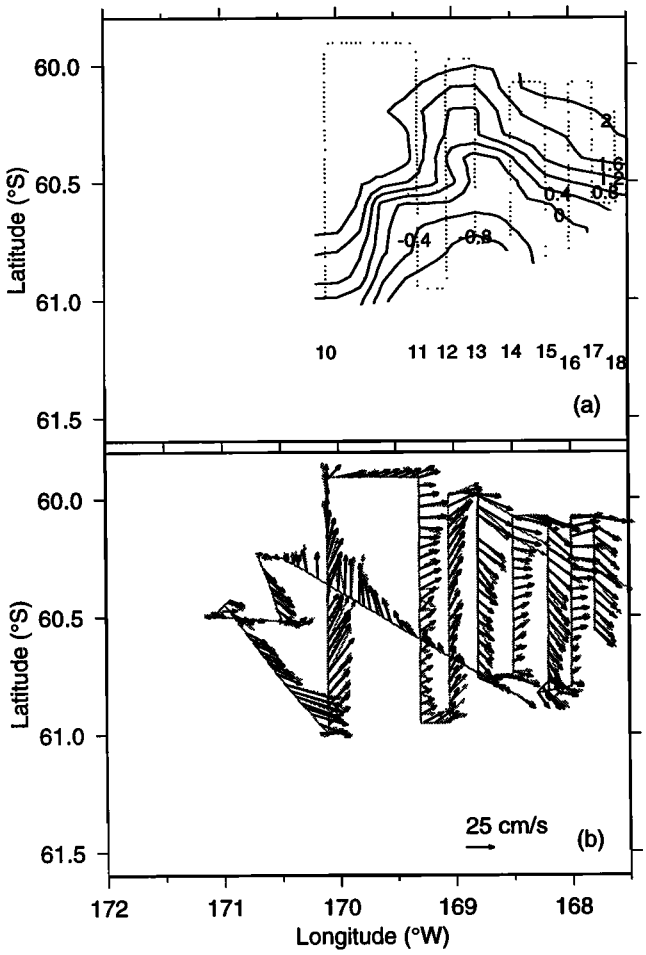

Figure 4. Maps from the second SeaSoar survey, November 15-19, 1997, of (a) surface temperature (°C) and (b) shipboard ADCP velocity averaged for 50-100 m (solid vectors) and for 200-300 m (shaded vectors). Data locations are shown as light dots in Figure 4a, and the ship track is superimposed in Figure 4b. Individual lines are numbered, and a scale arrow for velocity is in the lower left corner of Figure 4b.

lationship (Figure 6b). Higher-phytoplankton biomass was found within the PF, with the majority found poleward of the jet center (-30×10^2 m^2 s^{-1}) (Figure 6c) (note that in Figures 6c and 6d the stream function axis is such that south is on the left). Last, as evident in Figure 5, MLs are generally deeper on the northern side of the PF jet (Figure 6d). In summary, higher-phytoplankton biomass was found when the ML depth was $\lesssim 200$ m, but the distribution of ML depth and the high-biomass regions is dictated by the geometry of the PF and jet.

Conditions favorable for phytoplankton growth will depend upon the relationship between ML depth, solar irradiance, vertical attenuation of light, and critical depth [e.g., *Nelson and Smith,* 1991]. We have estimates of each these parameters and can use them to evaluate the potential for phytoplankton growth along the PF. As indicated in Figure 5, ML depths >200 m were common on the northern side of the PF, while ML depths <200 m (or even <100 m) were found on the southern side. Phytoplankton will exhibit net growth if mixed no deeper than a critical depth at which vertically integrated respiration is balanced by integrated photosynthesis [e.g., *Sverdrup,* 1953; *Nelson and Smith,* 1991]. We have used the reformulation developed by *Nelson and Smith* [1991] to calculate critical depths, applying our estimated values of K_{PAR}, surface PAR, and daily integrated irradiance (Table 2). We have used two different values for the net compensation irradiance, the best available estimate at the time of 35 μmol quanta m^{-2} s^{-1} used by *Nelson and Smith* [1991], and 10 μmol quanta m^{-2} s^{-1} as suggested from incuba-

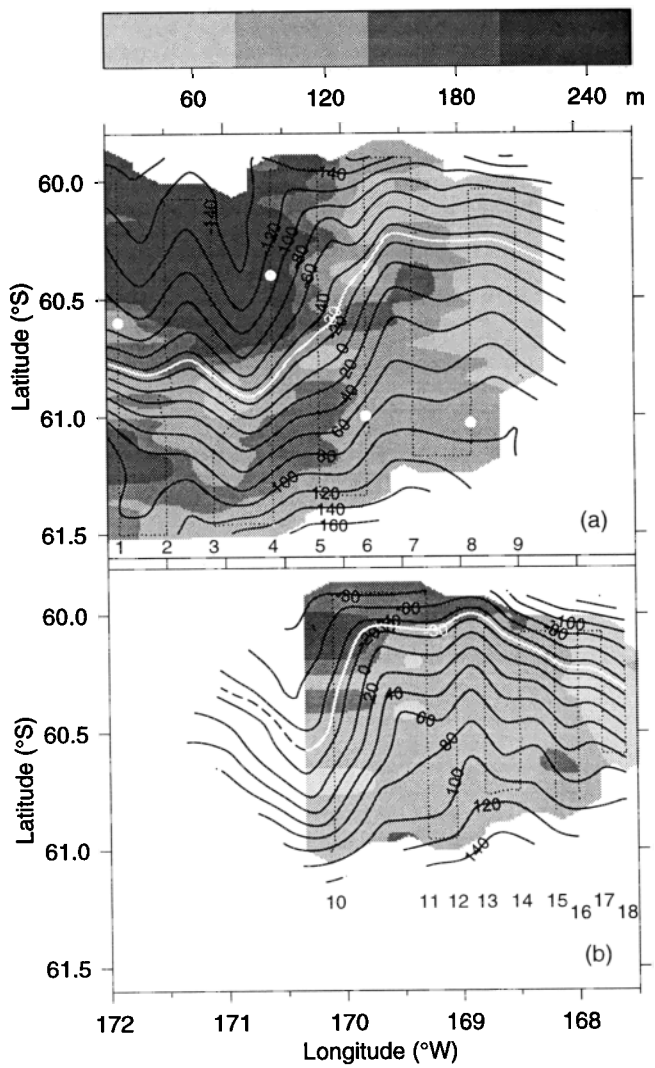

Figure 5. Maps of ML depth (m) using a $\Delta\sigma_t = 0.01$ kg m^{-3} criterion overplotted with contours of velocity stream function (10^2 m^2 s^{-1}) obtained from shipboard ADCP measurements averaged over 50-100 m: (a) November 7-12 and (b) November 15-19, 1997. The highlighted stream function contour indicates the center of the PF jet; white solid circles in Figure 5a indicate the locations where critical layer depths are estimated.

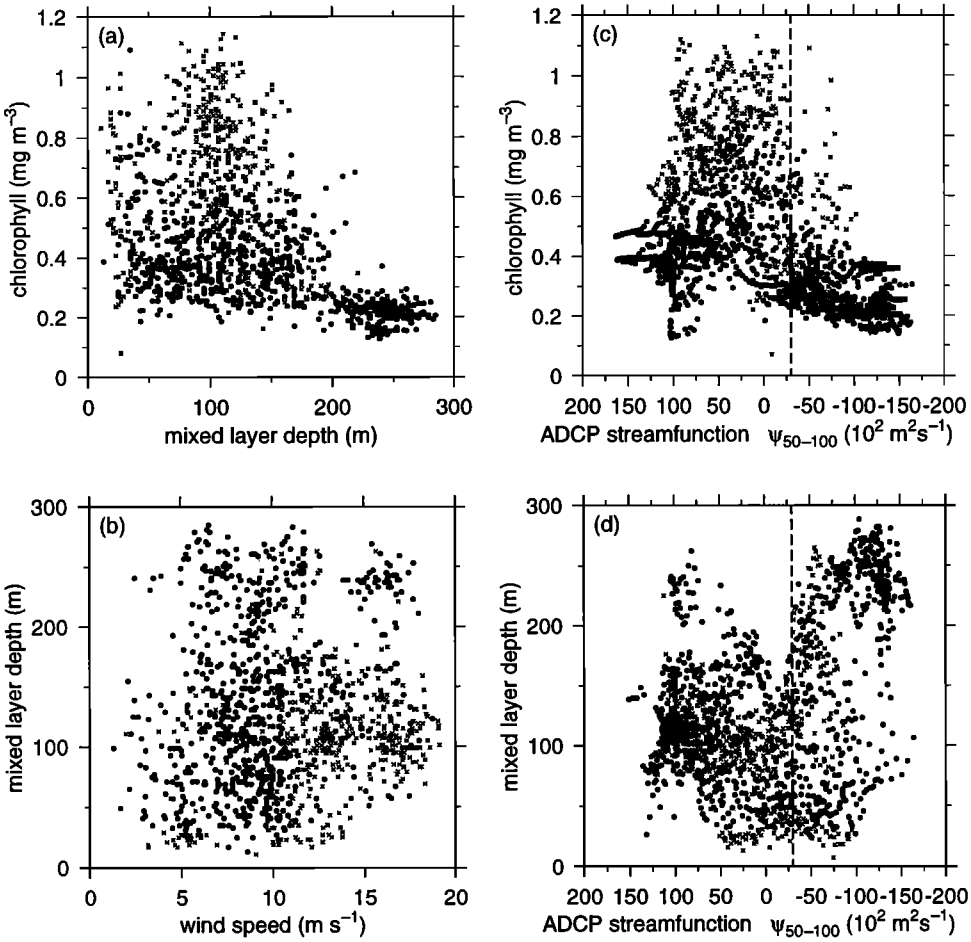

Figure 6. Scatterplots for data from the first SeaSoar survey, November 7-12, 1997 (solid circles), and the second SeaSoar survey, November 15-19, 1997 (crosses). Chlorophyll is from 51 m SeaSoar fluorescence data, and wind speed is as measured from the ship. The dashed lines in Figures 6c and 6d indicate the approximate location of the center of the PF jet.

tions conducted on this cruise by *Landry et al.* [this issue]. For specific locations along the SeaSoar survey lines of map 1 (Figure 5a), we tabulate daily integrated irradiance, surface irradiance, K_{PAR}, euphotic zone depth, and the two estimates of critical depth in relation to ML. Daily irradiance was <25 mol m^{-2} d^{-1} for much of our survey along lines 1-4, with an increase to 40 mol m^{-2} d^{-1} from lines 6 to 8. The increased daily irradiance and increased K_{PAR} (caused by higher-phytoplankton biomass) led to an increase in the estimated critical depth (Table 2). Note, however, that the assumption of the lower net compensation irradiance (10 μmol m^{-2} s^{-1} in Z_{cr_2} in Table 2) results in critical depths much deeper than the ML defined by the 0.01 kg m^{-3} criterion, while the 35 μmol m^{-2} s^{-1} assumption results in critical depths much shallower than the ML for locations on lines 1 and 4. *Landry et al.* [this issue] suggest that a net compensation irradiance value of 10 μmol m^{-2} s^{-1} may be appropriate for use in critical depth theory, consistent with *Boyd et al.*'s [1995] proposition that 5-10 μmol m^{-2} s^{-1} was valid for open Antarctic waters. Our results show that higher phytoplankton biomass is only found for MLs $\lesssim$200 m (Plate 2 and Figures 5 and 6), contrary to the prediction in Table 2 that growth should be positive for MLs as deep as 400 m (using 10 μmol m^{-2} s^{-1} net compensation irradiance). It is possible that the phytoplankton assemblage north of the PF had a net compensation irradiance >10 μmol m^{-2} s^{-1}, with corresponding shallower critical depths than indicated in Table 2. Spatial variability in trace metal limitation or nutrient availability across the PF zone [e.g., *Brzezinski et al.*, 2001] also could have contributed to the phytoplankton biomass differences in deep MLs north and south of the PF.

3.3. Temporal Variability

Time dependence of the physical and bio-optical fields has already been noted in conjunction with maps of surface temperature and ADCP velocity (Figures 3 and 4) and of ML chlorophyll (Plate 2) and ML depth (Figure 5). To illustrate further the change in the

Table 2. Estimates of Critical Depth Relative to Mixed Layer Depth for Selected Locations Near Maximum Solar Elevation (Local Noon) Along the Lines of the SeaSoar Survey Conducted November 7-12, 1997 (Map 1)

Line	Location	Year Day, UT	Daily[a] Irradiance I_0, mol m^{-2} d^{-1}	Surface[a] Irradiance E_0, μmol quanta m^2 s^{-1}	K^a_{PAR} m^{-1}	Euphotic[a] Zone, m (1% E_0)	$Z^b_{cr\_1}$, m	$Z^c_{cr\_2}$, m	ML Depth, m
1	60.60°S, 171.90°W	311.948	11	331	0.057	80	52	182	119
4	60.40°S, 170.60°W	313.961	23	519	0.050	93	120	421	257
6	61.00°S, 169.80°W	314.985	42	1558	0.061	75	183	641	93
8	61.03°S, 168.90°W	315.994	39	1508	0.064	72	162	567	75

[a]Derived from subsurface PAR profiles from PAR sensor on the SeaSoar vehicle.
[b]From (5), *Nelson and Smith* [1991], $Z_{cr} = 0.8 \times 11.57\ [I_0/(\mathrm{NCI})(K_{PAR})]$, where NCI is net compensation irradiance of 35 μmol m^{-2} s^{-1}.
[c]As above, with an NCI of 10 μmol m^{-2} s^{-1}.

physical fields between maps 1 and 2, the midpoints of which are separated by 7.5 days, contours of SST and 50-100 m average ADCP stream function are plotted in Figure 7. The meander in the PF propagated to the east. The translation of the cyclonic meander near 169°-170°W is evident in SST (Figure 7a), while the movement of the anticyclonic meander near 170°-171°W is best seen in ADCP stream function (Figure 7b). The eastward propagation velocity is estimated at 0.05-0.08 m s^{-1}, and the meander had an alongfront wavelength of ~175 km.

4. Discussion

We have presented several realizations of the phytoplankton biomass field in the PF region as observed with SeaSoar during austral spring. Vertical sections show 10-20 km wide bands of high chlorophyll on individual N-S transects (Plates 1f, 3c, 5c, and 6c). A horizontal map reveals coherent areas of high chlorophyll (Plate 2), but the smoothing required to produce sensible contours smears out the small-scale features measured with the SeaSoar's high along-track resolution. To emphasize the narrow bands making up the pools of high phytoplankton biomass and to investigate their continuity between north-south sections, we examined the concentration of chlorophyll at 51 m as a function of ADCP stream function for each north-south section (Figure 8). Nondivergent flow is along lines of constant ADCP stream function, so continuity between lines can be explored in this presentation (note that the stream function axis in Figure 8 is such that south is on the left). The west to east increase in chlorophyll to the south of the PF and jet in map 1 (Figure 8a) is apparent as is the fact that the high biomass consists of many narrow (10-15 km wide) bands. Alongstream continuity between the high-chlorophyll bands is evident, for example, along the stream function value 40×10^2 m^2 s^{-1} between lines 5 and 9 (see arrow in Figure 8a; see also Plate 2a where these locations are denoted with white circles). Although the degree of alignment is influenced by the estimate of flow streamlines, other narrow bands or tubes of high-phytoplankton biomass are apparent in Figure 8. Evidently, these narrow bands of high chlorophyll are common in the horizontally sheared PF jet, having also been observed in the Southern Polar Front in the Bellingshausen Sea near 85°W [*Pollard et al.*, 1995].

Further evidence for distinct narrow bands of high chlorophyll based on water mass distinctions was presented earlier (Plate 4). The presence of coherent bands between lines is also consistent with differential advection of a passive tracer in a horizontally sheared flow such as is found in the PF jet. The presence of these streaks argues against horizontal diffusion as the major cause of the widening of the area of high-phytoplankton biomass along the jet from west to east. Rather, the phytoplankton are growing throughout the region of observed high chlorophyll, although most likely at different rates, depending on their precise local environment. These hot spots of phytoplankton growth are then sheared into the observed streaks by the horizontal velocity gradients within the PF jet.

The ADCP velocity data provide the means to consider the role of advection in influencing the observed biomass distributions. Furthermore, advection may alias spatial distributions measured during the multiday SeaSoar surveys. To address these issues, the SeaSoar measurements are repositioned using velocities derived from the ADCP stream function to create a synoptic map. Chlorophyll concentrations are repositioned (i.e., advected) to the midpoint in time of map 1 (midday on November 10), revealing the influence of PF jet advection on the observed distributions (Plate 7a). The repositioned, synoptic map of the high-phytoplankton biomass feature shows that it is farther west (169°-169.5°W), slightly shorter in the along-stream direction (45 versus 50 km), and more circular (note the disappearance of the two upstream wisps of high chlorophyll along 169.4°W near 60.3° and 60.6°S) than in the non-

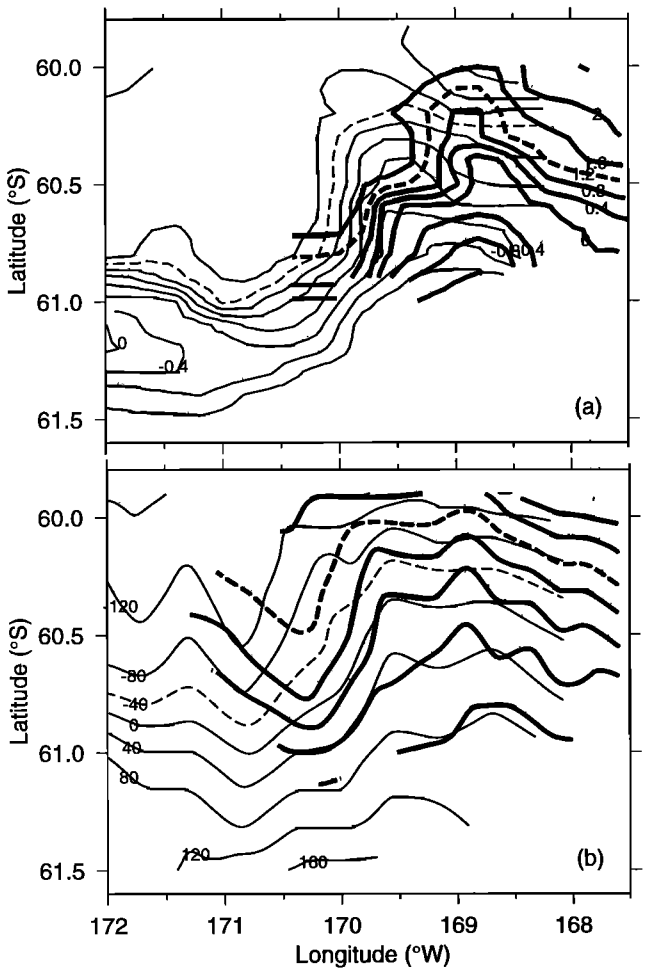

Figure 7. The time evolution between November 7-12 (thin contours) and November 15-19, 1997 (thick contours) for (a) surface temperature (°C) and (b) velocity stream function (10^2 m^2 s^{-1}) obtained from shipboard ADCP measurements averaged over 50-100 m. A selected contour in each panel is dashed to aid comparison between maps.

advected realization (Plate 2a). Advection of map 2 51 m chlorophyll to the midpoint of that survey (midday on November 17) shows similar effects, notably a reduction in alongfront extent from 120 to 80 km (note that these are lower bounds since the survey did not extend far enough east to delimit the high-chlorophyll biomass region) (Plate 7b).

It is important to note that the region of high-phytoplankton biomass has moved only slightly to the NE (center at 60.5°S, 169.25°W on November 10 compared with 60.3°S, 169.1°W on November 17), not some 100-200 km downstream as might be estimated from the PF jet speed over the 7 day interval. To illustrate that further, map 1 chlorophyll is advected using the map 2 stream function field to the midpoint in time of map 2 (Plate 7c). The region of high chlorophyll is located far to the east of the measured map 2 high-chlorophyll region (Plate 7b). Therefore the high biomass observed in map 2 centered at 60.3°S, 169.1°W is found in water advected from upstream; that is, this bloom consists of different phytoplankton than were observed a week earlier in map 1. If growth was occurring only within the water parcel in which high biomass was measured during map 1, we would not have observed a phytoplankton bloom at essentially the same location during both surveys. Advection of high biomass is certainly occurring, as hinted at by the elevated phytoplankton concentrations streaming off downstream (60.75°S, 168.25°W) as measured during map 2 (Plate 7b). Further evidence that high chlorophyll is found as a stream along the PF jet is found in the Sea-viewing Wide Field-of-view Sensor (SeaWiFS) surface chlorophyll images during this cruise and for an early summer period (November 3, 1997 to January 3, 1998) [*Moore et al.*, 1999b, Figure 1]. A key question is what causes the accumulated biomass to have a regional maximum at this particular location. One hypothesis is evaluated below. The shift to the NE in the high-chlorophyll region evident in the advected maps (Plate 7) is consistent with the shift in location of the cyclonic meander in the PF jet as revealed in SST (Figure 7).

To make an estimate of phytoplankton growth rate, we compute changes in chlorophyll concentration within the same water mass. The ADCP stream function is used to advect the maps 1 and 2 chlorophyll measurements to the locations they would have had at a common time, in this case, November 14, the midpoint between the two surveys. The advection algorithm is refined by using a stream function at each 15 min time step from a linear interpolation between the maps 1 and 2 stream functions (Plate 2). The stream function interpolation is done in the region of spatial overlap between maps 1 and 2. To choose the spatial extent of common coverage between the two repositioned maps, we translate to an alongstream distance–stream function coordinate system where the origin for the along stream distance is a line (60.0°S, 171.1°W to 61.5°S, 170.1°W) drawn approximately normal to the core of the PF jet at the western edge of the survey region. By comparing chlorophyll levels between specified stream function values and assuming nondivergent flow we assure that mass is conserved in the calculation. The region of overlap between maps 1 and 2 on November 14 spans stream function values of -100×10^2 to 90×10^2 m^2 s^{-1} and a distance of up to 110 km alongstream. Total chlorophyll in the overlap region in alongstream distance–stream function space, i.e., as measured 3.5 days earlier during map 1 and 3.5 days later during map 2, is vertically integrated over the SeaSoar depth range, including only values >0.20 mg m^{-3}. Since the SeaSoar measurements extend to well below the region of high chlorophyll (e.g., Plates 1f, 3c, 5c, and 9c), this integration gives a reliable estimate of chlorophyll in the water column. Given the uncertainty of the chlorophyll fluorescence measurements, we estimate the error

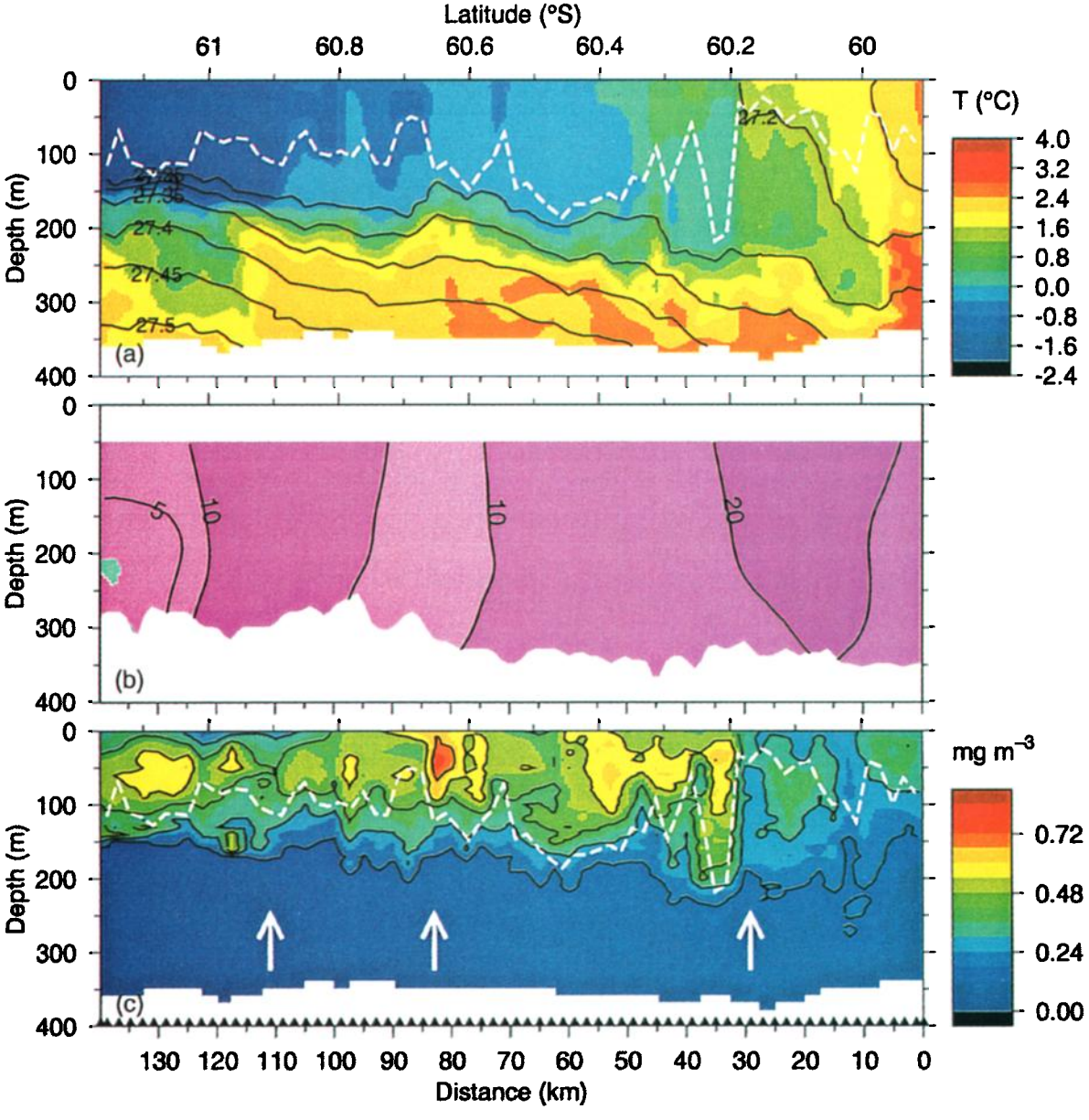

Plate 5. Vertical sections along 169.4°W (line 7) from 1017 to 2029 UTC, November 11, 1997, of (a) temperature overplotted with contours of density anomaly (kg m^{-3}), (b) shipboard ADCP east-west velocity (cm s^{-1}), and (c) chlorophyll. Individual 2 km vertical profiles from the SeaSoar measurements are indicated by solid triangles along the bottom of Plate 5c; ML depth is shown as a dashed white curve. White arrows in Plate 5c show the location of profiles used for T/S analysis (Plate 4b).

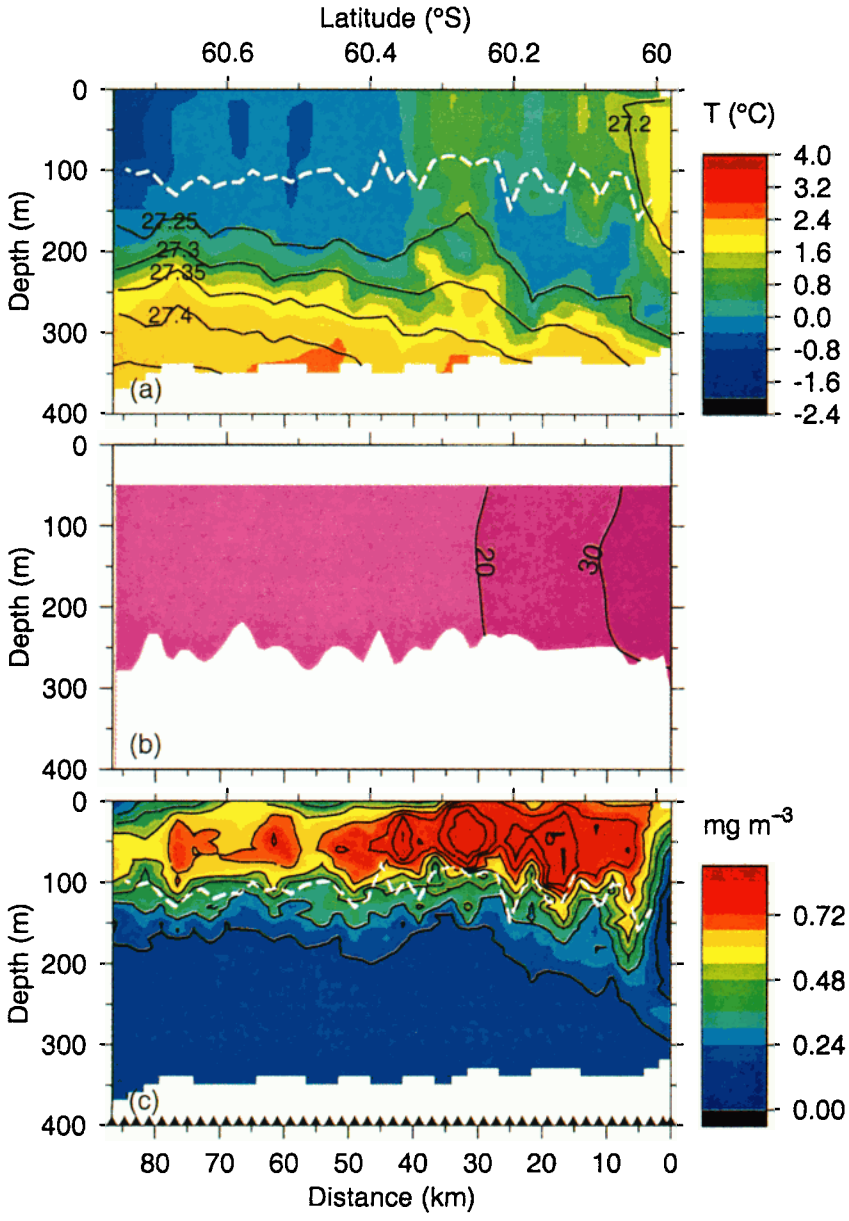

Plate 6. Vertical sections along 168.8°W (line 13) from 2007 UTC, November 16, to 0222 UTC, November 17, 1997, of (a) temperature overplotted with contours of density anomaly (kg m^{-3}), (b) shipboard ADCP east-west velocity (cm s^{-1}), and (c) chlorophyll. Individual 2 km vertical profiles from the SeaSoar measurements are indicated by solid triangles along the bottom of Plate 6c; ML depth is shown as a dashed white curve.

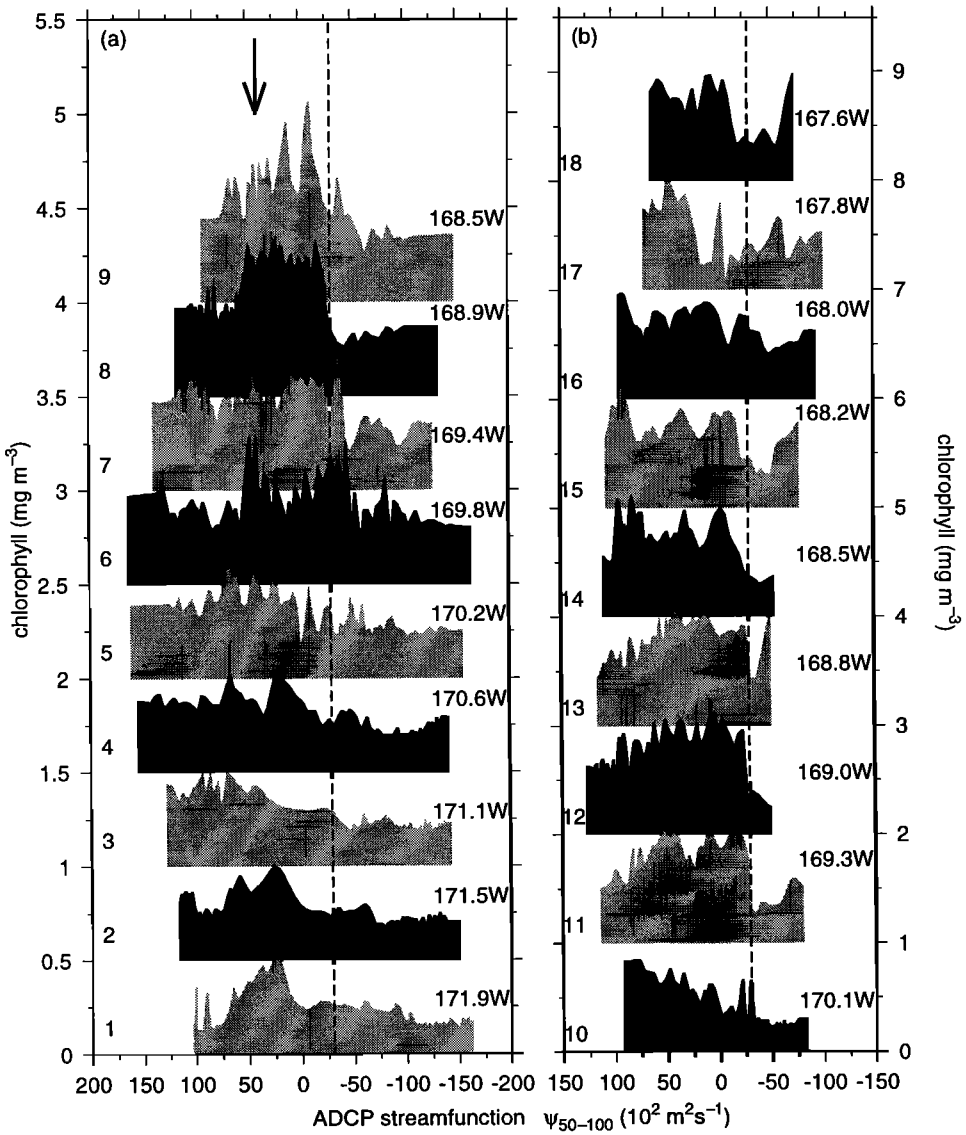

Figure 8. Chlorophyll at 51 m versus velocity stream function obtained from shipboard ADCP measurements averaged over 50-100 m. Data are from all lines (line numbers at left, as in Plate 2, corresponding to longitudes at right) during the two SeaSoar surveys in November 1997. Note the change in the chlorophyll scale between Figures 8a and 8b. Each profile has been offset along the ordinate by (a) 0.5 and (b) 1.0 mg m^{-3}. The dashed lines indicate the approximate location of the center of the PF jet and the arrow in Figure 8a shows the location of a thin, coherent chlorophyll streak stretching (at least) between lines 5 and 9, a distance of 120 km.

in growth rate to be 0.01 d^{-1}. By using the integrated chlorophyll between each map and the time between the midpoints of their occupation (7 days) an estimate of net growth rate is 0.05±0.01 d^{-1} or a net doubling time of 14 ± 3 days.

The net growth rate obtained from bottle incubations (0.04 d^{-1}) is within the error bars of our estimate and the rate from the net accumulation of phytoplankton biomass (0.03 d^{-1}) measured with bio-optical drifters is slightly smaller [*Landry et al.*, this issue]. The net in situ growth rate estimate of 0.08 d^{-1} based on surface phytoplankton carbon analysis [*Brown and Landry,* this issue] is higher than the chlorophyll-based estimates (0.03–0.05 d^{-1}). By adjusting for the change in carbon to chlorophyll ratios between the two maps, *Brown and Landry* [this issue] estimate a chlorophyll-based growth rate of 0.04–0.05 d^{-1}, comparable to the SeaSoar-based estimate.

The observed meander of the PF in this region is clearly an important feature. Its observed wavelength (175 km) and propagation speed (0.05-0.08 m s^{-1} eastward) in the direction of the mean flow is consistent with its origin from hydrodynamic instability of the PF jet [*McWilliams et al.*, 1978]. This meandering is the

mesoscale variability described in the ACC and PF from satellite observations [e.g., *Chelton et al.*, 1990] and modeling experiments [e.g., *McWilliams et al.*, 1978; *Ivchenko et al.*, 1997]. Mesoscale meandering of a front and jet causes localized areas of upwelling and downwelling as fluid parcels stretch or contract to preserve their potential vorticity. The upwelling and downwelling can, in turn, influence growth rates of ocean biota [e.g., *Flierl and Davis,* 1993] through changes induced in light levels and/or nutrient or trace metal fluxes. For the meander observed here, downwelling is expected upstream of the cyclonic bend (centered on 60.6°S, 169.9°W) and upwelling downstream (centered on 60.3°S, 169.0°W). We are determining the fields of vertical velocity from observed density and ADCP velocity fields via the quasi-geostrophic omega equation [*Hoskins et al.*, 1978]. Detailed results of this analysis will be reported elsewhere, but preliminary results support the location of the upwelling and downwelling centers along the meander as described above. However, the biological response to changes in light level or nutrient flux is not instantaneous so that it is not expected that the high-chlorophyll feature associated with the cyclonic meander observed near 60.3°S, 169°W is due to the enhanced meander-driven upwelling found at this location. Rather, with a 14 day net doubling time for phytoplankton within the PF the results of phytoplankton growth, perhaps stimulated by injection of micronutrients into the euphotic zone, should be located downstream from a meander-driven upwelling center. The observed chlorophyll levels at 60.3°S, 169°W represent approximately one doubling from the highest level observed upstream in the western part of the study region (0.4 mg m^{-3}) (line 1, Plate 2). At an average jet speed of 0.16 m s^{-1} the water parcel found in the region of highest chlorophyll was 195 km upstream 14 days earlier. This location, near 61°S, 171°W, is just downstream of the next cyclonic meander upstream, a region where locally enhanced upwelling is expected to occur and, in fact, is present in preliminary omega equation calculations. A faster average PF jet speed of 0.20 or 0.25 m s^{-1} would suggest that net growth rates could be higher, 0.06 or 0.08 d^{-1}, respectively, depending on spatial differences in grazing intensity [*Brown and Landry,* this issue]. Finally, it should be noted that upwelling of nutrients and/or trace metals via meander-driven upwelling results in a net vertical flux over a complete wavelength that also contains a downwelling region because of the presence of nonconservative mixing in the surface mixed layer.

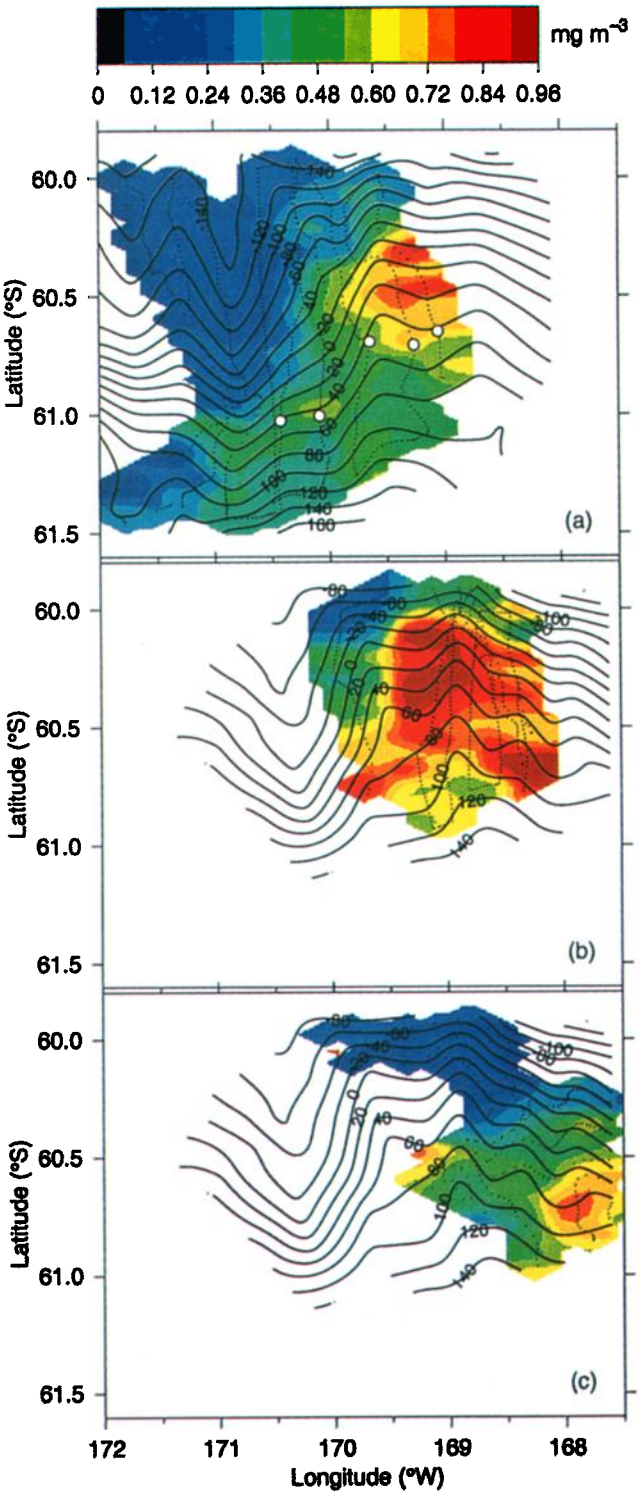

Plate 7. Maps of 51 m chlorophyll (mg m^{-3}) overplotted with contours of velocity stream function (10^2 m^2 s^{-1}) obtained from shipboard ADCP measurements averaged over 50-100 m. (a) As measured during November 7-12, 1997, but advected to midday on November 10 using velocities from the displayed ADCP stream function. (b) As measured during November 15-19, 1997, but advected to midday on November 17. (c) As measured during November 7-12, 1997, but advected to midday on November 17 using the stream function measured on November 15-19. Data locations after advection are shown as light dots. White solid circles in Plate 7a indicate the location of a chlorophyll streak along lines 5-9 (see Figure 8a).

We observed areas north and south of the PF in late October and early November that had relatively low phytoplankton biomass (0.20 mg m^{-3}) within the mixed layer (Plates 1f and 2). If we consider this to be a background biomass for the region, we can use our observations of the accumulation of phytoplankton biomass along the PF to estimate a date for initiation of phytoplankton growth in the area. We estimated a net accumulation rate of 0.05 d^{-1} along the axis of the PF during mid-November, with biomass values of 0.8 mg m^{-3} along the eastern side of map 1. *Landry et al.* [this issue] suggest an accumulation rate of 0.04 d^{-1}. Our data indicate that the phytoplankton in the mixed layer had gone through two doublings (net growth) by November 11-12. If the net growth had been constant during transit along the PF, two doublings at 0.05 d^{-1} yield 28 days since initiation of growth (biomass accumulation) above background concentrations, or 34 days using 0.04 d^{-1}. This calculation suggests that PF phytoplankton assemblages began net growth (the initiation of a spring bloom) between October 9 and 15.

These accumulation rates and bloom initiation dates allow estimates to be made of the distance traveled downstream in the PF by the phytoplankton assemblages prior to our observations. At 0.16 m s^{-1}, phytoplankton in the mixed layer will have traveled 390 or 470 km downstream, assuming a constant net accumulation rate during a 28 or 34 days transit.

At the southern end of our initial transect along 170°W on October 27 we detected increased phytoplankton biomass (0.35 mg m^{-3}) in the cold, low-salinity waters extending 100-150 km north of the ice edge (Plate 1f). If we apply the same range of net growth rates (0.04–0.05 d^{-1}) to this biomass, we obtain a starting date between October 13 and 16, similar to that estimated for the PF itself.

In summary, mesoscale meandering drives localized upwelling and the attendant nutrient and/or trace metal flux, to which phytoplankton growth responds and leads to regions with higher phytoplankton biomass some distance downstream dictated by mean advection speeds and phytoplankton growth rates. This downstream region of higher chlorophyll remains in place with respect to the meander and flow patterns and is continually supplied by phytoplankton that have been growing since upstream stimulation. Downstream of the high-chlorophyll region, it would be expected to see a stream of high-phytoplankton biomass as hinted at during map 2 and further suggested by SeaWiFS sea surface chlorophyll imagery, which shows a ribbon of high values along the PF [*Moore et al.*, 1999b]. It is important to note that the patterns of biomass distribution observed in the SeaSoar surveys are defined on a different timescale than those revealed in the composite SeaWiFS images analyzed by *Moore et al.* [1999b]. Because of the distribution of clouds in the PF region, *Moore et al.* [1999b] used weekly and monthly composite images to detect phytoplankton biomass patterns along the PF in November 1997. The spatial variability observed in the SeaSoar surveys would appear as more continuous bands of higher biomass in composite SeaWiFS images. Further exploration and quantification of the meander-driven upwelling and downwelling will appear in a forthcoming paper.

As suggested above, localized upwelling of micronutrients at particular locations along a meandering PF could create spatial variability in local growth rates and could result in the appearance of localized regions of higher biomass downstream (as seen in Plates 2 and 7). The size of these regional maxima and the spacing between successive maxima depend upon the interaction of several factors, including (1) the curvature of the meandering PF (thus altering the intensity of local upwelling and downwelling), (2) changes across the PF region in the depth of micronutrient concentrations adequate to stimulate growth, (3) variability in solar irradiance, and (4) variability in microzooplankton and mesozooplankton grazing. We observed up to fourfold fluctuations in daily irradiance over intervals of 1-2 days (Figure 1a), but we have insufficient temporal resolution of the other factors to evaluate adequately the relative contribution of these factors to the observed spatial structure of high-phytoplankton biomass through the PF region.

Although the initial N-S transect along 170°W (Plate 1) showed highest chlorophyll concentrations associated with low-salinity water presumably related to recent ice melt along the ice edge, the high-chlorophyll biomass feature that dominates the observations here spans a range of salinities. This is consistent with growth in open water conditions, perhaps via the meander-driven mechanism presented here. *Boyd et al.* [1995] also report a high-chlorophyll feature, which they suggest is initiated in open water. Thus, to the west of the cyclonic meander observed here, elevated chlorophyll values may be associated with an ice edge bloom [*Smith and Nelson,* 1986] but are relatively small compared with the large chlorophyll feature downstream. Spatial separation between an ice edge bloom and high chlorophyll at the PF was also noted by *Moore et al.* [1999b].

5. Conclusions

As part of the U.S. Southern Ocean JGOFS program, high-resolution hydrographic, velocity and bio-optical surveys of the Antarctic Polar Front were made during austral spring, October-November 1997. There was considerable mesoscale variability in both the physical and chlorophyll biomass fields, the latter estimated from calibrated fluorescence measured onboard the towed, undulating vehicle SeaSoar. In addition to horizontal maps and vertical sections of the various properties, temperature/salinity characteristics and nondivergent stream function derived from upper layer (50-100 m)

shipboard ADCP velocities were used to examine the influence of the physical fields on the distribution of chlorophyll biomass.

A north-south transect along 170°W in late October from north of the PF to the edge of the loose ice pack at 62.3°S showed that the PF was located at 60.35°-61.10°S and consisted of a SST drop from 1.6° to −1.6°C. By aligning the entire set of nearly orthogonal crossings of the front (13 sections), the PF was shown to have a width of around 100 km. Maximum eastward velocities in the PF jet were 0.4-0.5 m s^{-1}. To the north of the PF, mixed layers were deep (200-250 m), while south of the PF, they shoaled to 100-125 m. Low chlorophyll was found in general, with slightly elevated values (0.35 mg m^{-3}) south of the PF in cold, fresh surface water presumably influenced by ice melt. There were a number of 8-20 km wide cold features at 200-350 m beneath the PF and arrayed along the plunging frontal isopycnals, suggesting the subduction of cold, fresh Antarctic Surface Water.

A 200 by 150 km map revealed a large-amplitude meander in the PF. It had an alongfront wavelength of 175 km, a cross-front peak-to-peak amplitude of 100 km, and propagated to the east at 0.05-0.08 m s^{-1}. All these characteristics point toward its origin in hydrodynamic instability of the PF jet. Chlorophyll biomass was high (up to 1.1 mg m^{-3}) in a 50 by 50 km region to the south of the PF jet center and just downstream of the cyclonic bending portion of the meander. A second survey 7.5 days later showed growth of the phytoplankton biomass so that values in excess of 0.8 mg m^{-3} occupied a 80 km cross front by (at least) 80 km alongfront region. By using velocities from the nondivergent stream function to advect chlorophyll observations to a common time, the high-biomass feature was shown to be essentially growing in place with respect to the meander. It moved slightly (25 km) to the NE consistent with propagation of the meander over the week separating the midpoints of the two surveys. This contrasts with an alongstream distance of up to 100-130 km, which might be expected from advection with an average PF jet speed of 0.16-0.20 m s^{-1}.

Maps of mixed layer depth from the two surveys and scatterplots of mixed layer depth versus cross-front location (as denoted by stream function value) reveal deep (>200 m) mixed layers north of the PF and shallower (<140 m) mixed layers within and to the south of the PF. Elevated chlorophyll values were only found for mixed layers <200 m depth, consistent with estimates of the critical depth. However, no correlation was found between mixed layer depth and chlorophyll concentration, nor was there a simple relationship between wind speed and mixed layer depth. It was clear that the PF was most useful for delineating areas of differing mixed layer depths.

Phytoplankton biomass was organized in coherent, narrow bands along the PF. These 10-20 km wide bands of high chlorophyll had temperature-salinity properties distinct from adjacent water parcels and extended (at least) 120 km along the PF. These bands are likely due to differential advection within the horizontally sheared PF jet and provide support for the argument that horizontal diffusion is not primarily responsible for the increase in spatial extent of the region of high-chlorophyll biomass.

After adjusting for advection the spatial extent of common coverage between the two surveys was determined. From changes in estimates of integrated chlorophyll over 7 days, where the integration is both in the vertical and horizontally between two stream function contours so that mass is conserved, a net growth rate of 0.05 ± 0.01 d^{-1} was determined. Net growth rate estimates from bottle incubations and as observed by bio-optical drifters fall within the error bars of the SeaSoar-based estimate.

A hypothesis was evaluated to explain the observed spatial and temporal characteristics of the high-biomass feature. The large-amplitude meander of the PF drives localized upwelling through the conservation of potential vorticity. The resulting nutrient and/or trace metal vertical flux, to which phytoplankton growth responds, leads to a region of high chlorophyll a distance downstream dictated by mean advection speeds and phytoplankton growth rates. This region of high chlorophyll remains in place with respect to the meander pattern as it is continually fed by growing phytoplankton. Upwelling of nutrients and/or trace metals via meander-driven upwelling results in a net vertical flux over a complete wavelength that also contains a downwelling region because of the presence of nonconservative mixing in the upper mixed layer. Downstream of the high-chlorophyll region, a stream of high-phytoplankton biomass, as suggested by SeaWiFS sea surface chlorophyll imagery, is expected. Since mesoscale activity is common to the PF jet, the meander-driven process described here may have a strong influence on productivity within this major Southern Ocean feature.

Acknowledgments. Thanks to the Oregon State University Marine Technicians, J. M. Willis and L. Fayler, who were responsible for the highly successful SeaSoar operations. The officers and crew of the R/V *Roger Revelle* performed superbly. We thank R. O'Malley and C. Wingard for their efforts in data collection and processing and their assistance in analysis. This work was funded by National Science Foundation grant OPP-9530758. This paper is contribution 611 from the U.S. JGOFS program.

References

Abbott, M. R., J. G. Richman, R. M. Letelier, and J. S. Bartlett, The spring bloom in the Antarctic Polar Frontal Zone as observed from a mesoscale array of bio-optical sensors, *Deep Sea Res., Part II, 47*, 3285–3314, 2000.

Akima, H., Rectangular-grid-data surface fitting that has the accuracy of a bicubic polynomial, *Trans. Math. Software, 22*, 357–361, 1996.

Barnes, S. L., Applications of the Barnes objective analysis scheme, part III, Tuning for minimum error, *J. Atmos. Oceanic Technol.*, *11*, 1459–1479, 1994.

Barth, J. A., and D. J. Bogucki, Spectral light absorption and attenuation measurements from a towed undulating vehicle, *Deep Sea Res., Part I*, *47*, 323–342, 2000.

Barth, J. A., S. D. Pierce, and R. L. Smith, A separating coastal upwelling jet at Cape Blanco, Oregon and its connection to the California Current System. *Deep Sea Res., Part II*, *47*, 783–810, 2000.

Botnikov, V. N., Geographical position of the Antarctic Convergence Zone in the Southern Ocean (in Russian), *Sov. Antarct. Exped. Inf. Bull.*, *41*, 19–24, 1963. (*Sov. Antarc. Exped. Inf. Bull., Engl. Transl.*, *4*, 324–327, 1963.)

Boyd, P. W., C. Robinson, G. Savidge, and P. J. L. Williams, Water column and sea-ice primary production during austral spring in the Bellingshausen Sea, *Deep Sea Res., Part II*, *42*, 1177–1200, 1995.

Brainerd, K. E., and M. C. Gregg, Surface mixed and mixing layer depths, *Deep Sea Res., Part I*, *42*, 1521–1543, 1995.

Brown, S. L., and M. R. Landry, Mesoscale variability in biological community structure and biomass in the Antarctic Polar Front region at 170°W during austral spring 1997, *J. Geophys. Res.*, this issue.

Brzezinski, M. A., D. M. Nelson, V. M. Franck, and D. E. Sigmon, Silicon dynamics within an intense diatom bloom at the Antarctic Polar Front along 170°W Longitude, *Deep Sea Res., Part II*, in press, 2001.

Carter, E. F., and A. R. Robinson, Analysis models for the estimation of oceanic fields, *J. Atmos. Oceanic Technol.*, *4*, 49–74, 1987.

Chelton, D. B., M. G. Schlax, D. L. Witter, and J. G. Richman, Geosat altimeter observations of the surface circulation of the Southern Ocean, *J. Geophys. Res.*, *95*, 17,877–17,903, 1990.

Daley, R., *Atmospheric Data Analysis*, 457 pp., Cambridge Press, New York, 1991.

de Baar, H. J. W., J. T. M. de Jong, D. C. E. Bakker, B. M. Löscher, C. Veth, U. Bathmann, and V. Smetacek, Importance of iron for plankton blooms and carbon dioxide drawdown in the Southern Ocean, *Nature*, *373*, 412–415, 1995.

Flierl, G. R., and C. S. Davis, Biological effects of Gulf Stream meandering, *J. Mar. Res.*, *51*, 529–560, 1993.

Gille, S. T., and K. A. Kelly, Scales of spatial and temporal variability in the Southern Ocean, *J. Geophys. Res.*, *101*, 8759–8773, 1996.

Gordon, A. L., An Antarctic oceanographic section along 170°E, *Deep Sea Res., Part I*, *22*, 357–377, 1975.

Hawkins, H. F., and S. L. Rosenthal, On the computation of streamfunctions from the wind field, *Mon. Weather Rev.*, *93*, 245–252, 1965.

Herman, A. W., Simultaneous measurements of zooplankton and light attenuance with a new optical plankton counter, *Cont. Shelf Res.*, *8*, 205–221, 1988.

Hoskins, B. J., I. Draghici, and H. C. Davies, A new look at the ω-equation, *Q. J. R. Meteorol. Soc.*, *104*, 31–38, 1978.

Huntley, M. E., M. Zhou, and W. Nordhausen, Mesoscale distribution of zooplankton in the California Current in late spring, observed by optical plankton counter, *J. Mar. Res.*, *53*, 647–674, 1995.

Huyer, A., J. A. Barth, P. M. Kosro, R. K. Shearman, and R. L. Smith, Upper-ocean water mass characteristics of the California current, summer 1993, *Deep Sea Res., Part II*, *45*, 1411–1442, 1998.

Ivchenko, V. O., A. M. Treguier, and S. E. Best, A kinetic energy budget and internal instabilities in the Fine Resolution Antarctic Model, *J. Phys. Oceanogr.*, *27*, 5–22, 1997.

Joyce, T. M., On in situ calibration of shipboard ADCPs, *J. Atmos. Oceanic Technol.*, *6*, 169–172, 1989.

Joyce, T. M., and S. L. Patterson, Cyclonic ring formation at the Polar Front in the Drake Passage, *Nature*, *265*, 131–133, 1977.

Kosro, P. M., Shipboard acoustic profiling during the Coastal Ocean Dynamics Experiment, Ph.D thesis, *SIO Ref. 85-8*, Scripps Inst. of Oceanogr., La Jolla, Calif., 1985.

Landry, M. R., S. L. Brown, K. E. Selph, M. R. Abbott, R. M. Letelier, S. Christensen, R. R. Bidigare, and K. Casciotti, Initiation of the spring phytoplankton increase in the Antarctic Polar Front Zone at 170°W, *J. Geophys. Res.*, this issue.

McWilliams, J. C., W. R. Holland, and J. H. S. Chow, A description of numerical Antarctic Circumpolar Currents, *Dyn. Atmos. Oceans*, *2*, 213–291, 1978.

Moore, C. C., J. R. V. Zaneveld, and J. C. Kitchen, Preliminary results from an in-situ spectral absorption meter, Ocean Optics XI, *Proc. SPIE Int. Soc. Opt. Eng.*, *1750*, 330–337, 1992.

Moore, J. K., M. R. Abbott, and J. G. Richman, Location and dynamics of the Antarctic Polar Front from satellite sea surface temperature data, *J. Geophys. Res.*, *104*, 3059–3073, 1999a.

Moore, J. K., M. R. Abbott, J. G. Richman, W. O. Smith, T. J. Cowles, K. H. Coale, W. D. Gardner, and R. T. Barber, SeaWiFS satellite ocean color data from the Southern Ocean, *Geophys. Res. Lett.*, *26*, 1465–1468, 1999b.

Nelson, D. M., and W. O. Smith Jr., Sverdrup revisited: Critical depths, maximum chlorophyll levels, and the control of Southern Ocean productivity by the irradiance-mixing regime, *Limnol. Oceanogr.*, *36*, 1650–1661, 1991.

Nowlin, W. D., Jr., and J. M. Klinck, The physics of the Antarctic Circumpolar Current, *Rev. Geophys.*, *24*, 469–491, 1986.

Orsi, A. H., T. Whitworth III, and W. D. Nowlin Jr., On the meridional extent and fronts of the Antarctic Circumpolar Current, *Deep Sea Res., Part I*, *42*, 641-673, 1995.

Patterson, S. L., Surface circulation and kinetic energy distribution in the Southern Hemisphere oceans from FGGE drifting buoys, *J. Phys. Oceanogr.*, *15*, 865–884, 1985.

Pierce, S. D., J. A. Barth, and R. L. Smith, Improving acoustic Doppler current profiler accuracy with wide-area differential GPS and adaptive smoothing of ship velocity, *J. Atmos. Oceanic Technol.*, *16*, 591–596, 1999.

Pollard, R., Frontal surveys with a towed profiling conductivity/temperature/depth measurement package (SeaSoar), *Nature*, *323*, 433–435, 1986.

Pollard, R. T., J. F. Read, J. T. Allen, G. Griffiths, and A. I. Morrison, On the physical structure of a front in the Bellingshausen Sea, *Deep Sea Res., Part II*, *42*, 955–982, 1995.

Schaefer, J. T., and C. A. Doswell, On the interpolation of a vector field, *Mon. Weather Rev.*, *107*, 458–476, 1979.

Schwiderski, E. W., Global ocean tides, part II, The semidiurnal principal lunar tide (M2), in *Atlas of Tidal Charts and Maps, Tech. Rep. TR 79-414*, 87 pp., Naval Surf. Weapons Cent., Dahlgren, Va., 1979.

Smith, W. O., and D. M. Nelson, Importance of ice edge phytoplankton production in the Southern Ocean, *BioScience*, *36*, 251–257, 1986.

Strass, V. H., A. C. Naveira Garabato, R. T. Pollard, H. Fischer, I. Hense, J. T. Allen, J. F. Read, H. Leach, and V. Smetacek, Mesoscale frontal dynamics: Shaping the environment of primary production in the Antartic Circumpolar Current, *Deep Sea Res., Part II*, in press, 2001.

Sverdrup, H. U., On conditions for the vernal blooming of

phytoplankton, *J. Cons. Int. Explor. Mer.*, *18*, 287–295, 1953.

Turner, D. R., and N. J. P. Owens, A biogeochemical study in the Bellingshausen Sea: Overview of the STERNA 1992 expedition, *Deep Sea Res., Part II*, *42*, 907–932, 1995.

Western Environmental Technology Laboratories (WET Labs), Inc., FlashPak user's guide, internal report, 16 pp., Philomath, Oregon, 1997.

Wilson, D., and A. Leetma, Acoustic Doppler current profiling in the equatorial Pacific in 1989, *J. Geophys. Res.*, *93*, 13,947–13,966, 1988.

Wunsch, C., and D. Stammer, The global frequency-wavenumber spectrum of oceanic variability from TOPEX/Poseidon altimetric measurements, *J. Geophys. Res.*, *100*, 24,895–24,910, 1995.

J. A. Barth, T. J. Cowles, and S. D. Pierce, College of Oceanic and Atmospheric Sciences, Oregon State University, 104 Ocean Administration Building, Corvallis, OR 97331-5503. (barth@oce.orst.edu)

(Received December 15, 1999; revised December 6, 2000; accepted December 11, 2000.)